Metabolic Engineering 77 (2023) 256–272

Contents lists available at ScienceDirect

Metabolic Engineering

journal homepage: www.elsevier.com/locate/meteng

Implantation of CPT1AM-expressing adipocytes reduces obesity and glucose intolerance in mice

M Carmen Soler-Vázquez [a], María del Mar Romero [a,b,1], Marijana Todorcevic [a,1], Katia Delgado [a], Carles Calatayud [c,d], Aleyda Benitez -Amaro [e,f], Maria Teresa La Chica Lhoëst [e,f,g], Paula Mera [a,b], Sebastián Zagmutt [a], Marianela Bastías-Pérez [a], Kevin Ibeas [a,b], Núria Casals [b,h], Joan Carles Escolà-Gil [f,i], Vicenta Llorente-Cortés [e,f,j], Antonella Consiglio [c,d,k], Dolors Serra [a,b], Laura Herrero [a,b,*]

[a] Department of Biochemistry and Physiology, School of Pharmacy and Food Sciences, Institute of Biomedicine of the University of Barcelona (IBUB), Universitat de Barcelona (UB), E-08028, Barcelona, Spain
[b] Centro de Investigación Biomédica en Red (CIBER) de Fisiopatología de la Obesidad y Nutrición (CIBEROBN), Instituto de Salud Carlos III, E-28029, Madrid, Spain
[c] Department of Pathology and Experimental Therapeutics, Bellvitge University Hospital- IDIBELL, E-08908, Hospitalet de Llobregat, Barcelona, Spain
[d] Institute of Biomedicine of the University of Barcelona (IBUB), Universitat de Barcelona, E-08028, Barcelona, Spain
[e] Lipids and Cardiovascular Pathology, Institut d'Investigacions Biomèdiques de Barcelona (IIBB-CSIC), 08041, Barcelona, Spain
[f] Institut d'Investigació Biomèdica Sant Pau (IIB SANT PAU), 08041, Barcelona, Spain
[g] Universitat Autònoma de Barcelona, Spain
[h] Basic Sciences Department, Faculty of Medicine and Health Sciences, Universitat Internacional de Catalunya (UIC), E-08195, Sant Cugat del Vallés, Barcelona, Spain
[i] CIBER de Diabetes y Enfermedades Metabólicas Asociadas (CIBERDEM), 28029, Madrid, Spain
[j] CIBER of Cardiovascular (CIBERCV), Instituto de Salud Carlos III, E-28029, Madrid, Spain
[k] Department of Molecular and Translational Medicine, University of Brescia, Piazza del Mercato, 15, 25121, Brescia, BS, Italy

ARTICLE INFO

Keywords:
Obesity
Type 2 diabetes
Adipose tissue
Adipose tissue-derived mesenchymal stem cells
Carnitine palmitoyltransferase 1A

ABSTRACT

Obesity and its associated metabolic comorbidities are a rising global health and social issue, with novel therapeutic approaches urgently needed. Adipose tissue plays a key role in the regulation of energy balance and adipose tissue-derived mesenchymal stem cells (AT-MSCs) have gained great interest in cell therapy. Carnitine palmitoyltransferase 1A (CPT1A) is the gatekeeper enzyme for mitochondrial fatty acid oxidation. Here, we aimed to generate adipocytes expressing a constitutively active CPT1A form (CPT1AM) that can improve the obese phenotype in mice after their implantation. AT-MSCs were differentiated into mature adipocytes, subjected to lentivirus-mediated expression of CPT1AM or the GFP control, and subcutaneously implanted into mice fed a high-fat diet (HFD). CPT1AM-implanted mice showed lower body weight, hepatic steatosis and serum insulin and cholesterol levels alongside improved glucose tolerance. HFD-induced increases in adipose tissue hypertrophy, fibrosis, inflammation, endoplasmic reticulum stress and apoptosis were reduced in CPT1AM-implanted mice. In addition, the expression of mitochondrial respiratory chain complexes was enhanced in the adipose tissue of CPT1AM-implanted mice. Our results demonstrate that implantation of CPT1AM-expressing AT-MSC-derived adipocytes into HFD-fed mice improves the obese metabolic phenotype, supporting the future clinical use of this *ex vivo* gene therapy approach.

1. Introduction

Obesity is a risk factor for several associated metabolic pathologies such as insulin resistance, type 2 diabetes (T2D), dyslipidemia, cardiovascular disease and even cancer (O'Neill and O'Driscoll, 2015). The pathophysiology of obesity-induced metabolic complications includes several mechanisms such as chronic low-grade inflammation, oxidative stress, mitochondrial dysfunction, impaired angiogenesis,

* Corresponding author. Department of Biochemistry and Physiology School of Pharmacy and Food Sciences, University of Barcelona Av. Joan XXIII, 27-31, E-08028, Barcelona, Spain.
E-mail address: lherrero@ub.edu (L. Herrero).
[1] Equal contribution.

https://doi.org/10.1016/j.ymben.2023.04.010
Received 23 June 2022; Received in revised form 14 February 2023; Accepted 16 April 2023
Available online 22 April 2023

hypoxia and cell death (de Mello et al., 2018; Herold and Kalucka, 2021). Despite the alarming global increase in the incidence of obesity and its associated metabolic diseases, current conventional methods such as surgical or pharmacological interventions combined with a healthy diet and lifestyle are limited by their poor long-term effectiveness, side effects and surgical risks (Williams et al., 2020). Thus, there is an urgent need for novel therapeutic approaches.

Mesenchymal stem cells (MSCs) are of great interest for their clinical application in cell therapy since they are found in most adult tissues, have a high capacity for tissue regeneration, can be isolated and expanded *in vitro*, and lack the ethical issues associated, for instance, with embryonic stem cells (Dominici et al., 2006). MSCs are characterized by (1) being able to be isolated and maintained as adherent cells in culture, (2) to express specific membrane markers including CD29, CD90 and Sca1 (and the absence of others such as CD34 and CD45) and (3) being able to differentiate into several lineages such as adipocytes, osteoblasts and chondrocytes (Dominici et al., 2006). MSCs can be isolated from different sources such as peripheral blood, bone marrow, placenta, gingival tissue and the umbilical cord, among others (Mushahary et al., 2017). However, recent investigations have highlighted that adipose tissue (AT) is the most appropriate source of MSCs in the study of obesity and other metabolic dysfunctions since it is widely distributed, is easily accessible (*i.e.*, less invasive isolation method), has a greater capacity for adipocyte differentiation and contains large numbers of MSCs per gram of tissue (Kolaparthy et al., 2015; Silva and Baptista, 2019).

AT plays a key role in regulating important metabolic pathways such as energy balance, glucose and lipid metabolism, hormones, and inflammation. AT can be classified into energy-storing white adipose tissue (WAT) and brown adipose tissue (BAT), which is specialized in the maintenance of body temperature by dissipating energy in the form of heat through non-shivering thermogenesis (Cannon and Nedergaard, 2004). A third type of adipocytes, beige or brite, has been described to have a role in adaptative thermogenesis. Beige adipocytes arise from a reversible process called browning or beiging, *i.e.*, the transition of white-into-beige adipocytes in response to cold temperatures or β-adrenergic stimuli. The browning process is characterized by increased mRNA levels of uncoupling protein 1 (UCP1). UCP1 is highly expressed in BAT, where it generates heat by uncoupling electron transport from ATP production. Metabolically active BAT is found in adult humans, with its activity inversely correlating with age, glucose levels and body mass index (van Marken Lichtenbelt et al., 2009; Nedergaard et al., 2007; Hany et al., 2002; Virtanen et al., 2009; Cypess et al., 2009; Zingaretti et al., 2009; Saito et al., 2009). Therefore, any strategy that can enhance the mass or activity of thermogenic fat might be of great interest to burn excessive lipids and combat obesity and its associated metabolic disorders.

Carnitine palmitoyltransferase 1 (CPT1) is the rate-limiting enzyme in mitochondrial fatty acid oxidation (FAO). It catalyzes the transport of long-chain fatty acids (FAs) inside the mitochondria so they can be oxidized to produce ATP, CO_2 or ketone bodies. There are three isoforms of CPT1 (CPT1A, CPT1B and CPT1C) showing different tissue distributions and sensitivity to their physiological inhibitor malonyl-CoA, which is mainly derived from glucose metabolism and is the first intermediate in FA synthesis (Serra et al., 2013; Casals et al., 2016). Interestingly, our group has generated a permanently active mutant form of CPT1A (CPT1AM) that is insensitive to malonyl-CoA, thus allowing continuous FAO independently of glucose levels (Morillas et al., 2003). CPT1AM is especially relevant in obesity, which usually shows high levels of both lipids and glucose. Importantly, individuals with obesity and T2D show lower FAO rates and WAT CPT1 mRNA and protein levels (Houmard, 2008; Kelley et al., 2002; Ritov et al., 2005; Simoneau et al., 1999). This prompted our group and others to modulate CPT1A expression *in vitro* and *in vivo* to combat obesity and T2D (Herrero et al., 2005a; Sebastián et al., 2007; Perdomo et al., 2004; Gao et al., 2011; Orellana-Gavaldà et al., 2011; Weber et al., 2020; Malandrino et al., 2015; Calderon-Dominguez et al., 2016a; Mir et al., 2018; Monsénégo et al., 2012; Stefanovic-Racic et al., 2008; Bruce et al., 2009).

In the search for new lipid-burning anti-obesity approaches, elegant studies have described several thermogenic activators in the last decade (Calderon-Dominguez et al., 2016a; Bastías-Pérez et al., 2020; Gavaldà-Navarro et al., 2022). Recent studies have tested interesting therapeutic approaches that directly increase thermogenesis by the implantation of BAT, AT-MSCs or beige adipocytes differentiated from preadipocytes, AT-MSCs or induced pluripotent stem cells (iPSCs) showing an improvement of the obese phenotype (Soler-Vázquez et al., 2018; Calvo et al., 2021; Silva et al., 2014; Lee et al., 2017; Kishida et al., 2015; Min et al., 2016; Thoonen et al., 2016; Chen et al., 2018). These are all relevant approaches. However, here we aimed to include several modifications: (1) we used CPT1AM-expressing AT-MSC-derived adipocytes to enhance the lipid-burning power and (2) since WAT is more accessible than BAT in humans, we decided to isolate AT-MSCs from subcutaneous inguinal WAT (iWAT), thereby increasing the translational potential of our approach for clinical cell therapy in humans.

Here, we describe for the first time that the subcutaneous implantation of CPT1AM-expressing AT-MSC-derived adipocytes into the dorsal area of mice fed a high-fat diet (HFD) reduces body weight, hyperglycemia, insulin resistance, serum cholesterol levels and hepatic steatosis. The implantation can also restore HFD-induced alterations in the expression of genes involved in lipid metabolism and oxidative damage in the liver, mitochondrial activity and apoptosis in WAT, and thermogenesis in BAT. This sheds light on a novel pre-clinical cell-based therapy for obesity and associated diseases.

2. Results

2.1. MSCs could be isolated from the gWAT, iWAT and iBAT of lean or obese mice and showed MSC-specific characteristics

AT-MSCs were isolated from lean or HFD-treated obese mice from different fat depots (iWAT, gonadal WAT (gWAT) and interscapular BAT (iBAT)) (Fig. 1, S1 and S2). MSCs isolated from the iWAT of lean mice (Fig. 1A) were differentiated into adipocytes (Fig. 1B and C), osteoblasts (Fig. 1D) and chondrocytes (Fig. 1E), thus proving their multipotency. Oil Red O staining revealed multiple intracellular lipid droplets in AT-MSC-derived adipocytes on day 12 of differentiation (Fig. 1C). iWAT-derived MSCs expressed MSC-specific cell surface markers such as CD90, CD105, CD29 and Sca1 (Fig. 1F). To evaluate whether the AT-MSC-derived adipocytes from iWAT maintained their beige or brown adipocyte signature, the expression of specific gene markers was analyzed. Beige adipocytes differentiated from iWAT-derived MSCs expressed beige- and BAT-specific markers such as *Tmem26* and *Ucp1*, respectively (Fig. 1G). Similar results were obtained when AT-MSCs were isolated from the gWAT or iBAT of lean mice in terms of multipotency (Fig. S1A-E, G-J) and the expression of cell surface markers (Fig. S1F). Beige adipocytes originating from gWAT-derived MSCs expressed the beige-specific marker (*Tmem26*) or the BAT-specific marker (*Ucp1*) only when incubated with the β3-receptor agonist (CL-316,243) (Fig. S1K). Brown adipocytes differentiated from iBAT-derived MSCs expressed BAT-specific markers (*Zic1* and *Ucp1*; Fig. S1L).

MSCs were also isolated from the iWAT of obese and hyperglycemic mice (Fig. S2). HFD-fed mice showed increases in body weight and glucose levels that reached statistical significance starting at 4 weeks after HFD treatment (Figs. S2A and S2B). iWAT-derived MSCs showed MSC-specific characteristics since they could differentiate into adipocytes, osteoblasts, and chondrocytes (Figs. S2C–G), expressed MSC-specific surface markers (Fig. S2H) and expressed beige- or BAT-specific markers when differentiated into beige adipocytes (Fig. S2I). To further characterize the differentiation of iWAT-derived MSCs from obese mice into adipocytes, both lipid content and the mRNA levels of adipogenic markers were evaluated during the differentiation period (0, 3, 6, 9 and 12 days) (Fig. S3). Oil Red O staining indicated an increase in

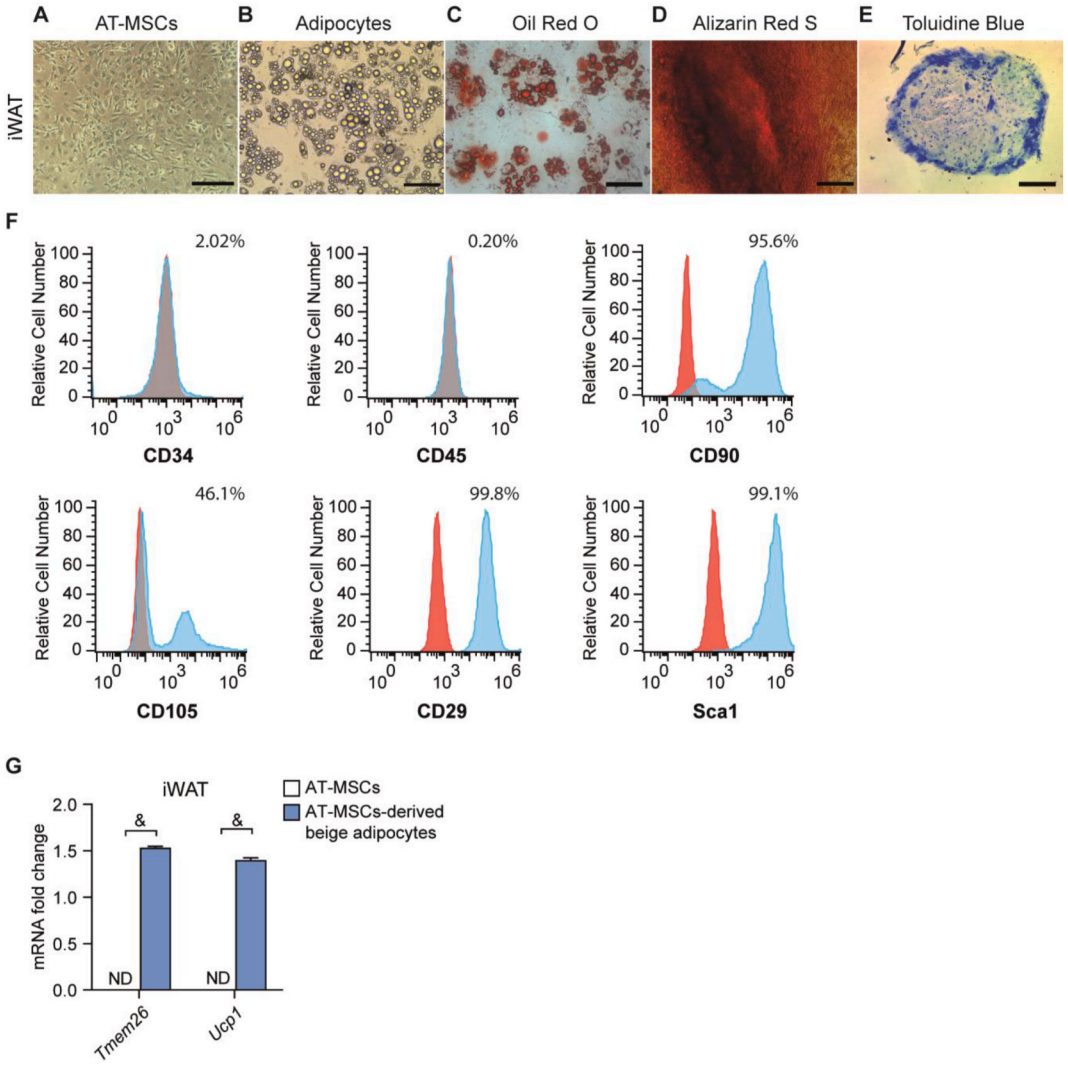

Fig. 1. Isolation and characterization of iWAT-isolated AT-MSCs from adult lean mice. (A) AT-MSCs on day 5 of culture. (B) Adipocytes on day 12 of differentiation. (C) Oil Red O staining on day 12 of adipogenic differentiation. (D) Alizarin Red S staining on day 21 of osteogenic differentiation. (E) Toluidine blue staining on day 30 of chondrogenic differentiation. Scale bar, 100 μm (magnification 20x). (F) Representative flow cytometry analysis of MSC cell surface markers (negative: CD34, CD45; positive: CD90, CD105, CD29 and Sca1) in iWAT-isolated AT-MSCs (red histogram represents isotype controls). (G) Relative expression of *Tmem26* and *Ucp1* in iWAT-isolated control AT-MSCs and those differentiated into beige adipocytes. Data are expressed as the mean ± SEM (n = 3–4). $^{\&}p < 0.0001$. ND, not detected.

the accumulation of triglycerides (TGs) in the lipid droplets on day 9 (Figs. S3A and S3B). However, differentiation markers were expressed earlier. Fatty acid binding protein 4 (*Fabp4*) and *Adiponectin* mRNA levels were increased starting on day 3 of differentiation, while the expression levels of peroxisome proliferator-activated receptor (*Ppar*) g, *Adipsin* and sterol regulatory element binding protein 1c (*Srebp1c)* were enhanced starting on day 6 (Fig. S3C). The mRNA levels of the negative adipogenic marker preadipocyte factor 1 (*Pref1)* were reduced from day 3 (Fig. S3C).

Altogether, these results indicated that MSCs were able to be isolated from the iWAT, gWAT and iBAT of lean or obese and hyperglycemic mice (Table S2). However, for subsequent transplantation experiments, iWAT-derived MSCs from adult lean mice were used. This decision was based on the following reasons: 1) When considering a potential therapeutic application in humans, the subcutaneous WAT (scWAT) is more accessible and its dissection less invasive than that of the visceral WAT or BAT, when a surgical resection such as liposuction or bariatric surgery is performed; and 2) although we were able to isolate, characterize and differentiate AT-MSCs from HFD-fed obese and hyperglycemic mice, it has been reported that advanced age or obesity promotes a senescent state of these cells and abnormal adipogenic differentiation (Mastrolia et al., 2019; Hass et al., 2011; Conley et al., 2020; Liu et al., 2017; Kornicka et al., 2018; Hristov et al., 2019; Fijany et al., 2019; Barbagallo et al., 2017; Rennert et al., 2014).

2.2. Lentivirus-mediated expression of CPT1AM in AT-MSC-derived adipocytes

iWAT-derived MSCs were differentiated into adipocytes (day 6) and transduced with a self-inactivating lentiviral vector (LV) expressing a bicistronic cassette encoding for CPT1AM, an internal ribosomal entry site (IRES) and GFP (LV-CPT1AM). Both LV-GFP or uninfected adipocytes were used as controls. The correct LV infection was confirmed by fluorescence emission (Fig. 2A), and the expression of CPT1AM by qRT-PCR (Fig. 2B) and Western blot (Fig. 2C and D). CPT1A protein levels were increased up to three-fold in the LV-CPT1AM-infected adipocytes compared to both non-transduced or LV-GFP transduced adipocytes (Fig. 2D). Consistent with the protein expression results, CPT1AM-expressing adipocytes showed both higher CPT1 activity and total FAO (Fig. 2E and F).

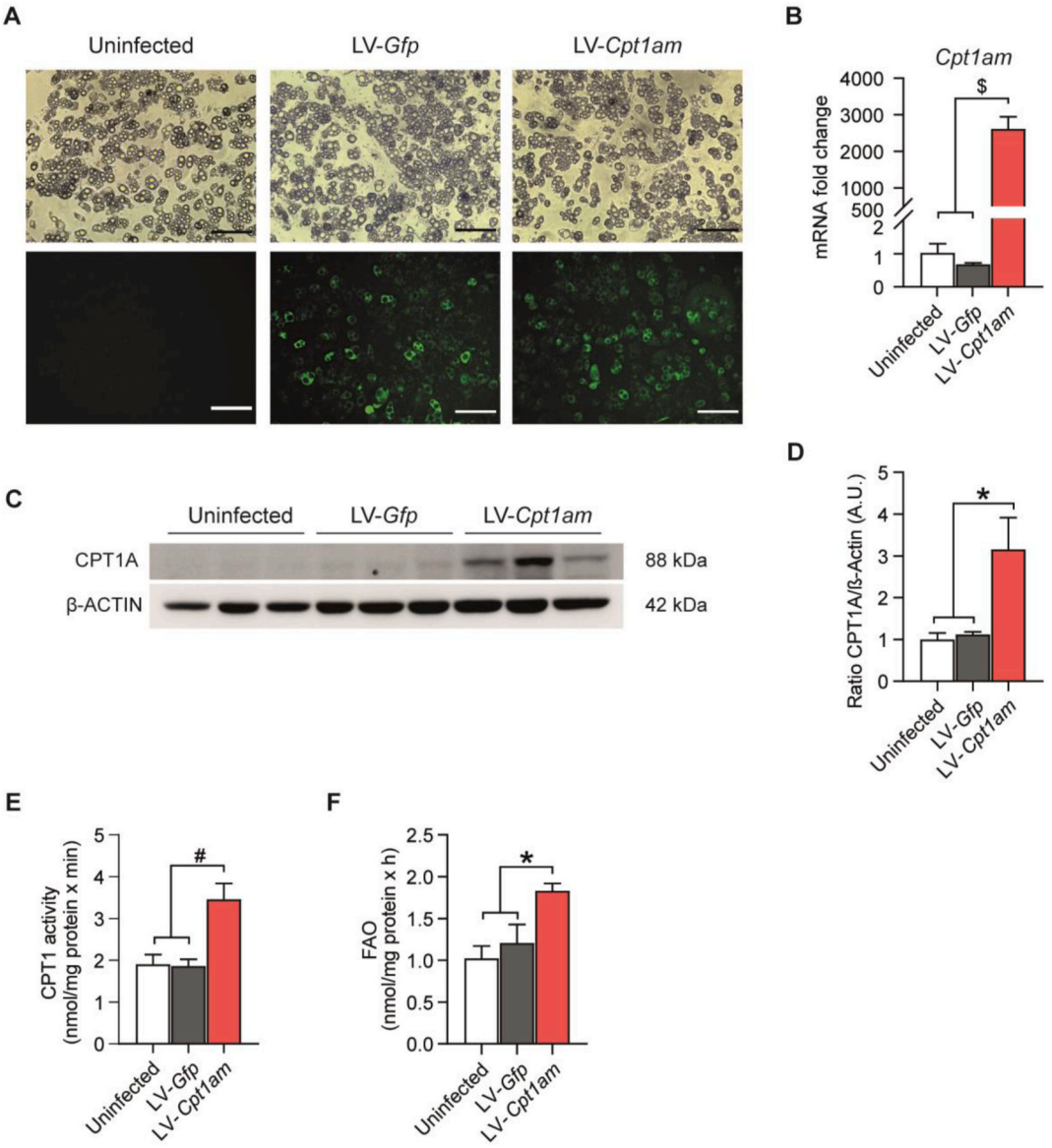

Fig. 2. CPT1AM expression in AT-MSC-derived adipocytes. (A) Representative images of iWAT-isolated MSC-derived adipocytes from adult lean mice under white light (top) and fluorescence emission in green (bottom) after transduction with LV-GFP or LV-CPT1AM at 10 MOI (multiplicity of infection) or not infected on day 6 of differentiation. Scale bar, 200 μm. (B) Relative *Cpt1am* mRNA levels. Western blot for CPT1A protein expression (C) and relative quantification (D). (E) CPT1A activity. (F) Total FAO represented as the sum of acid soluble products plus CO_2 oxidation. Data are expressed as the mean ± SEM (n = 3). *p < 0.05, #p < 0.01, $ p < 0.001.

2.3. *HFD CPT1AM-implanted mice showed reduced body weight, glucose intolerance, and insulin and cholesterol levels*

MSC-derived adipocytes from the iWAT of adult lean mice were infected with LV-GFP or LV-CPT1AM (GFP and CPT1AM, respectively), embedded in Matrigel and subcutaneously implanted into the dorsal area of mice. Implanted mice were fed an HFD or a normal chow diet (NCD) as a control.

To analyze whether the implantation of adipocytes *per se* might have had an effect on the HFD-induced phenotype, we compared HFD mice implanted with GFP-expressing AT-MSC-derived adipocytes or only with Matrigel (HFD GFP and HFD MG, respectively) (Fig. S4). No differences were seen in body weight, food intake, fasting blood glucose levels or the glucose tolerance test (GTT) (Figs. S4A–D). Thus, subsequent experiments were performed using GFP-implanted mice on the HFD as controls.

Starting at five weeks after the implantation, CPT1AM-implanted mice showed a lower body weight compared to the HFD GFP controls, without differences in food intake (Fig. 3A and B). HFD-induced increases in fasting blood glucose, insulin and leptin levels were reverted in the CPT1AM-implanted mice (Fig. 3C, D, F). Importantly, HFD-induced glucose intolerance was improved in the CPT1AM-implanted mice (Fig. 3E). While no differences were seen in the serum levels of lipids and lipoproteins with a high turnover such as TGs, very low-density lipoprotein (VLDL) + low-density lipoprotein (LDL) cholesterol or non-esterified fatty acids (NEFAs), HFD-induced increases in serum cholesterol, high-density lipoprotein (HDL) cholesterol and glycerol were blunted in the CPT1AM-implanted mice (Fig. 3G-L).

The presence and morphology of the implanted adipocytes embedded in Matrigel were studied at the end of the experiments (Fig. 4). Ten weeks after the transplantation, the implant was correctly located subcutaneously in the dorsal region of mice injected with the cell suspensions (Fig. 4A). Adipocytes were histologically found at the implants of the GFP- or CPT1AM-implanted mice (Fig. 4B) and those

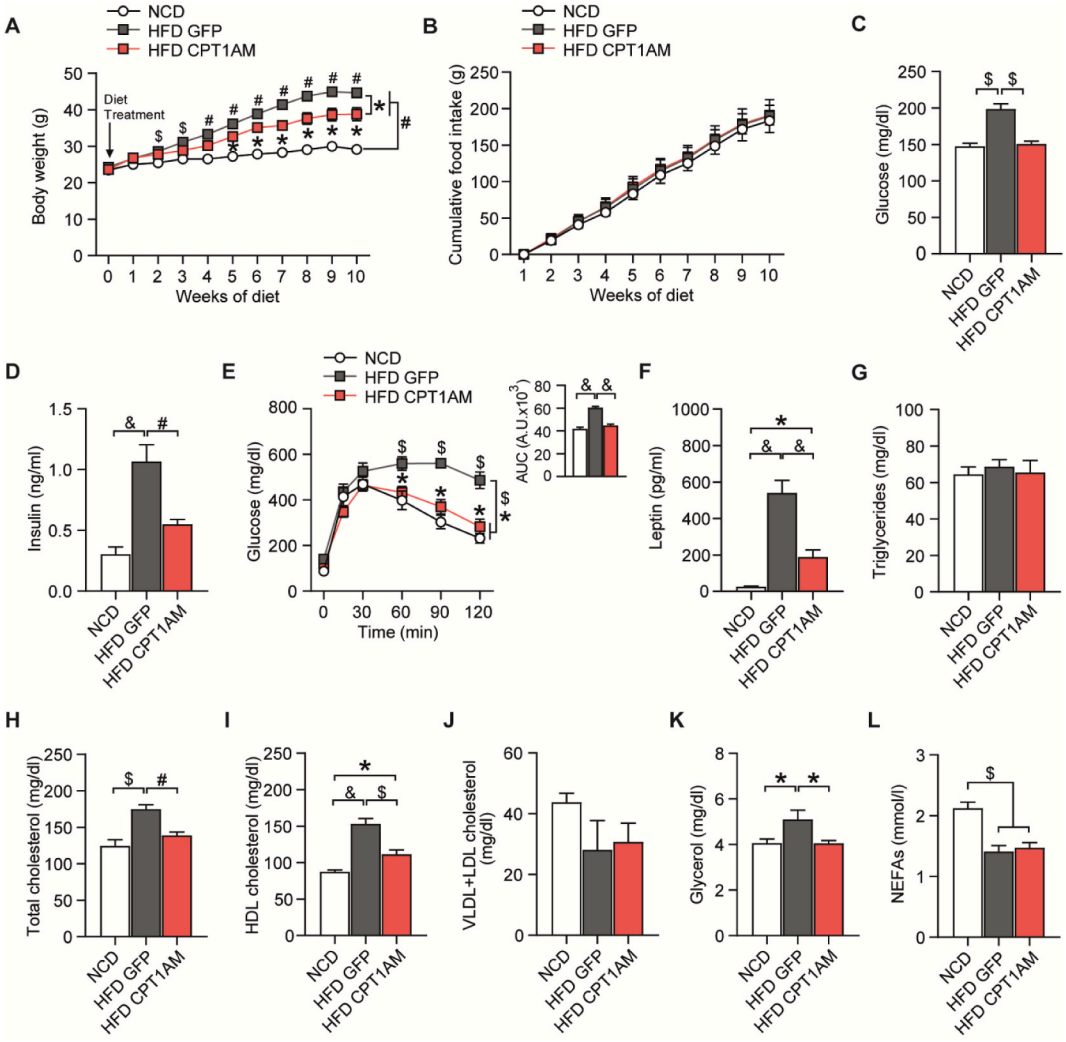

Fig. 3. CPT1AM-implanted mice showed reduced body weight, glucose intolerance, and serum insulin and cholesterol levels. AT-MSC-derived adipocytes from the iWAT of adult lean mice were infected with LV-GFP or LV-CPT1AM and subcutaneously implanted into the dorsal area of mice (week 0). Transplanted mice were fed an HFD or NCD as a control. Body weight (A) and food intake (B) were measured for 10 weeks after implantation. (C) Glucose levels 4 weeks after implantation. (D) Fasting serum insulin levels. (E) Glucose tolerance test (GTT) 9 weeks after implantation (right graph, area under the curve (AUC) for the GTT). Fasting serum leptin (F), triglyceride (G), total, HDL and VLDL + LDL cholesterol (H–J), glycerol (K) and non-esterified fatty acids (NEFAs, L) levels 10 weeks after implantation. Data are expressed as the mean ± SEM (n = 6–7). *p < 0.05 for HFD GFP *vs.* HFD CPT1AM, $p < 0.05 for NCD *vs.* HFD GFP, #p < 0.05 for NCD *vs.* HFD GFP or HFD CPT1AM. *p < 0.05, #p < 0.01, $ p < 0.001, &p < 0.0001.

present in the CPT1AM-implanted mice showed higher *Cpt1a* mRNA levels, as expected, compared with the HFD GFP controls (Fig. 4C). CPT1AM-expressing implants showed higher mRNA levels of thermogenic genes such as PR domain containing 16 (*Prdm16*), a transcription factor involved in brown adipocyte differentiation, and peroxisome proliferator-activated receptor γ co-activator 1 alpha (*Pgc1a*) the principal regulator of mitochondrial biogenesis, compared with the HFD GFP controls, while bone morphogenetic protein 8b (*Bmp8b*) didn't reach statistical significance (Fig. 4C). *Ucp1* was not detected (data not shown). No differences were seen in the other genes such as *Gfp*, *Cpt1b*, hormone sensitive lipase (*Hsl*), acetyl-CoA carboxylase (*Acc*) *2*, *Pparg*, *Leptin*, vascular endothelial growth factor A (*Vegfa*), transforming growth factor beta (*Tgfb*), arginase 1 (*Arg1*), interleukin (*Il*) 10 and apoptosis (*Caspase 3*) (Fig. 4C). The mRNA levels of other inflammatory genes such as *Il1b*, *Il6* or tumour necrosis factor alpha (*Tnfa*) were not detectable (data not shown). Consistently, histology showed no differences in the infiltration of immune cells such as macrophages or T cells or in apoptosis between the GFP and CPT1AM implants (Fig. 4D).

2.4. CPT1AM-implanted mice on an HFD showed reduced hepatic steatosis and oxidative stress and improved lipid, glucose and cholesterol metabolism

Ten weeks after the implantation, CPT1AM-implanted mice showed a reduction in HFD-induced hepatic steatosis (Fig. 5A and B, and Fig. S5A). Next, the mRNA levels of genes involved in lipid metabolism were studied in liver (Fig. 5C). HFD-induced alterations in *Hsl* (a lipolytic enzyme), *Acc1* (involved in malonyl-CoA synthesis and *de novo* lipogenesis), stearoyl-CoA desaturase 1 (*Scd1*) (promotes the desaturation of saturated FAs), diacylglycerol acyltransferase (*Dgat*) *1* (catalyzes the conversion of diacylglycerol into TGs) and *Ucp2* were reverted in the CPT1AM-implanted mice (Fig. 5C). No changes were observed in the mRNA levels of other genes such as the fatty acid transporter *Cd36* or perilipin (*Plin*) *2* (Fig. 5C). HFD-induced derangements were not different between CPT1AM- and GFP-implanted mice for the hepatic *Cpt1a* (Fig. 5C).

Next, the expression of hepatic genes involved in glucose and cholesterol metabolism were analyzed (Fig. 5D and E). The mRNA levels of the glucose transporter *Glut2* showed a 2.5-fold increase in the HFD

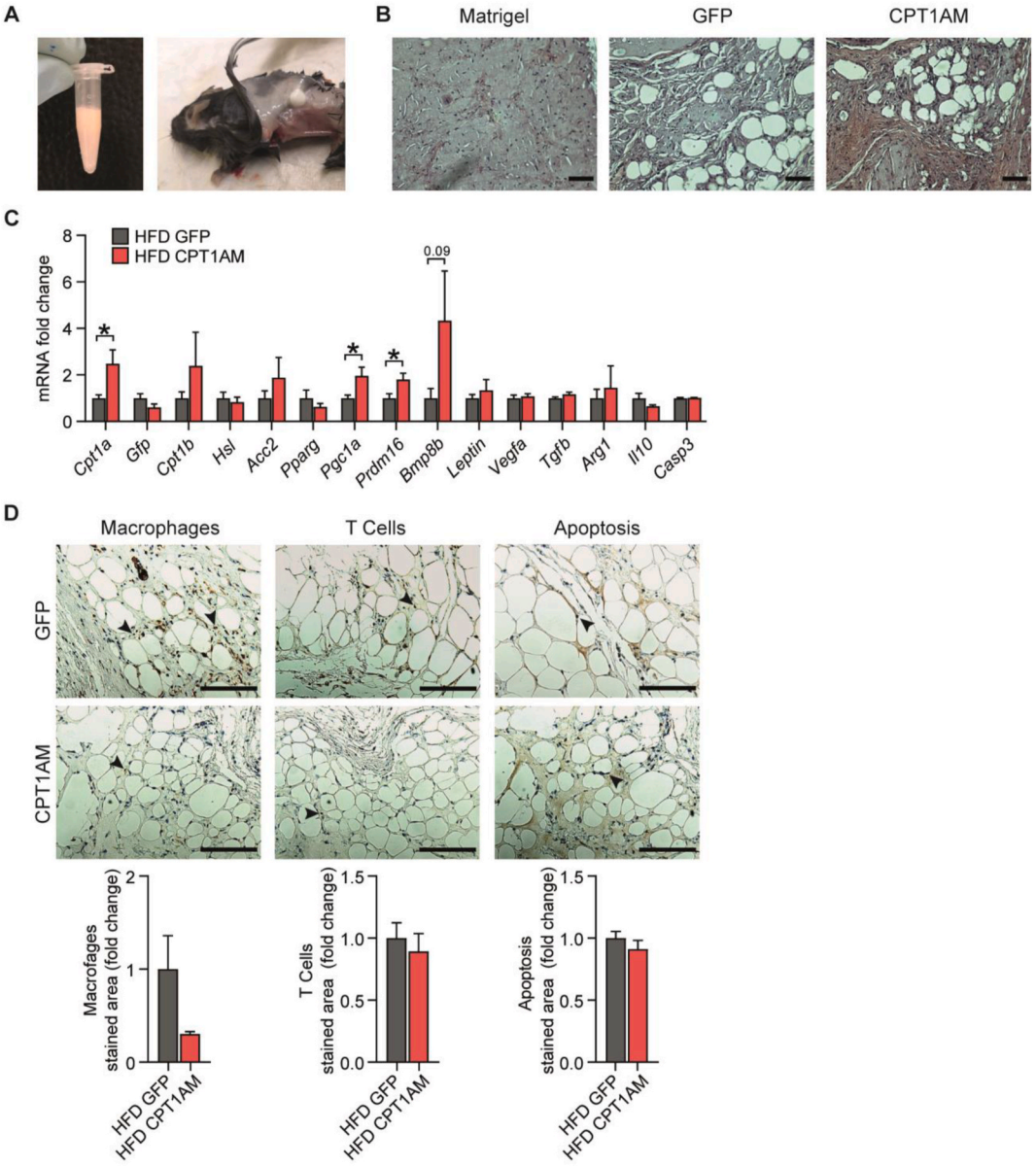

Fig. 4. Analysis of implanted adipocytes. (A) Suspension of infected adipocytes with Matrigel (left) and the dorsal area of a representative mouse injected with AT-MSC-derived adipocytes 10 weeks after the implantation (right). (B) Representative images of implant sections stained with H&E at the end of the experiments: Matrigel (left), GFP-implanted mice (middle) and CPT1AM-implanted mice (right). Scale bar, 100 μm. (C) Gene expression in implants of GFP- or CPT1AM-implanted mice fed an HFD (HFD GFP and HFD CPT1AM, respectively) for 10 weeks. (D) Immunohistochemical staining for macrophages (anti-Mac2), T cells (anti-CD3) and apoptosis (anti-Caspase3). Arrowhead indicates positive staining. Data are expressed as the mean ± SEM (n = 4–6). *p < 0.05.

CPT1AM mice compared to both the NCD and HFD GFP control mice (Fig. 5D). Interestingly, the HFD-induced decrease in the gluconeogenic gene glucose 6 phosphatase (*G6p*) mRNA levels was reverted in the CPT1AM-implanted mice (Fig. 5D). No changes were seen in phospho-enolpyruvate carboxykinase (*Pepck*) expression levels between the HFD GFP and HFD CPT1AM groups (Fig. 5D). HFD-induced increase in the glycolytic gene glucokinase (*Gck*) mRNA levels was reduced in the CPT1AM-implanted mice (Fig. 5D). HFD-induced alterations in the mRNA levels of cholesterol-related genes such as the ATP-binding cassette A 1 (*Abca1*) transporter, low-density lipoprotein receptor (*Ldlr*) and hydroxymethylglutaryl-CoA synthase (*Hmgcs2*; the enzyme involved in the first step of cholesterol synthesis) were reverted in the CPT1AM-implanted mice (Fig. 5E). No changes between the HFD GFP and HFD CPT1AM groups were seen in the expression level of HMG-CoA reductase (*Hmgcr*) (Fig. 5E). The analysis of the local lipid profile in the liver showed that CPT1AM-expressing mice had higher free cholesterol levels compared to NCD-treated controls (Fig. S5B). This is consistent with the higher Hmgcr mRNA levels observed in the HFD CPT1AM-expressing mice compared to NCD controls (Fig. 5E).

Hepatic mRNA levels of genes involved in the different ER stress-specific pathways as well as the inflammatory genes and enzymes involved in oxidative damage were analyzed (Fig. 5F). HFD-induced alterations in nitric oxide synthase 2 (*Nos2*), *Catalase*, glutathione peroxidase 3 (*Gpx3*), *Mcp1* and *Tnfa* were reverted in the CPT1AM-implanted mice (Fig. 5F). The mRNA level of the endoplasmic reticulum (ER) stress marker protein disulfide isomerase (*Pdi*) was reduced in the CPT1AM-implanted mice compared to the GFP controls on an HFD (Fig. 5F). No differences between the HFD GFP and HFD CPT1AM groups were seen in other genes such as immunoglobulin heavy-chain-binding protein (*Bip*), C/EBP homologous protein (*Chop*), ER degradation-enhancing alpha-mannosidase-like protein (*Edem*), superoxide dismutase (*Sod*), macrophage galactose-type lectin-1 (*Mgl1*), *Il10*,

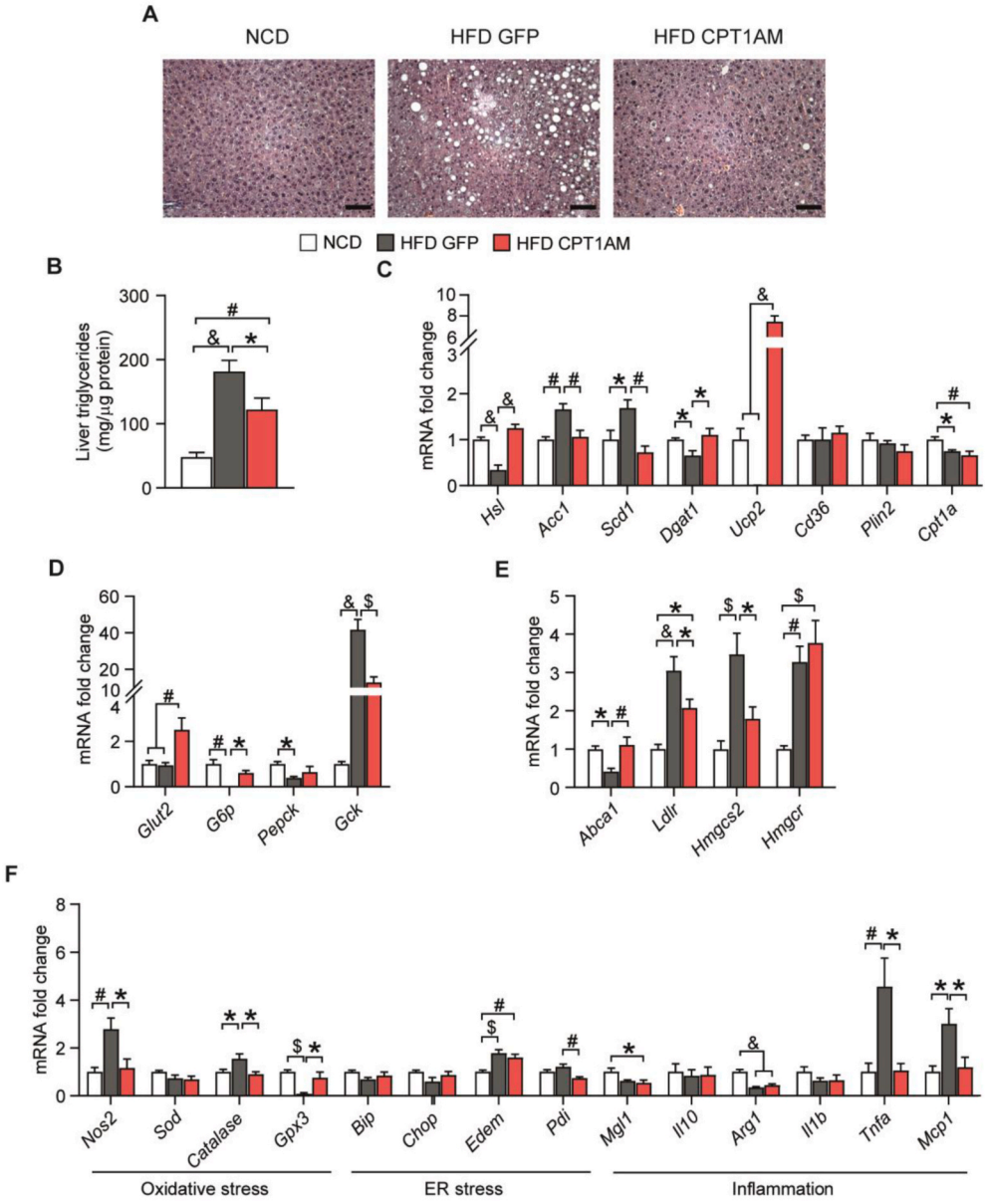

Fig. 5. Implantation of AT-MSC-derived adipocytes expressing CPT1AM reduced hepatic steatosis and restored lipid, glucose and cholesterol metabolism and ameliorated oxidative stress in HFD-fed mice. (A) Representative images of liver sections stained with H&E 10 weeks after implantation. Scale bar, 100 µm. (B) Liver triglyceride content quantification. mRNA levels of the genes involved in lipid metabolism (*CD36, Hsl, Plin2, Acc1, Scd1, Dgat1, Cpt1a* and *Ucp2*) (C); glucose metabolism (*Glut2, G6p*, *Pepck* and *Gck*) (D); cholesterol metabolism (*Abca1, Ldlr, Hmgcs2* and *Hmgcr*) (E); endoplasmic reticulum stress (*Bip, Chop*, *Edem* and *Pdi*), oxidative stress (*Nos2, Sod, Catalase* and *Gpx3*) and inflammation (*Il-1b*, *Mgl1, Il10* and *Arg1*) (F). Data are expressed as the mean ± SEM (n = 6–7). $^{*}p < 0.05$, $^{\#}p < 0.01$, $^{\$}p < 0.001$, $^{\&}p < 0.0001$.

Arg1, and *Il1b* (Fig. 5F).

2.5. CPT1AM-expressing adipocytes implantation improved hypertrophy, fibrosis, mitochondrial dysfunction, ER stress, apoptosis and inflammation in iWAT from HFD-fed mice

Ten weeks after the implantation, CPT1AM-implanted mice showed a 48.34% reduction in the iWAT weight compared to the HFD GFP group (NCD: 0.228 g ± 0.019; HFD GFP: 1.504 g ± 0.087; HFD CPT1AM: 0.777 g ± 0.094; Fig. 6A). Accordingly, histological analysis indicated a 47.89% decrease in the average adipocyte size of HFD CPT1AM mice compared to HFD GFP controls (Fig. 6B top panels, C). Morphometric analysis of the adipocyte distribution frequency revealed that adipocytes from the HFD CPT1AM mice were clustered in smaller sizes compared to those from the HFD GFP group (Fig. 6D). Since adipocyte hypertrophy and fibrosis are usually related to extracellular matrix (ECM) remodeling and/or hypoxia, we next evaluated collagen deposition with Masson's trichrome staining and genes related to these pathways in the implanted mice. HFD-induced increase in fibrosis was blunted in CPT1AM-expressing mice (Fig. 6B bottom panels, E). Consistently, HFD-induced alterations in the mRNA levels of collagen type I and IV alpha 1 (*Col1a1, Col4a1*), metalloproteinases 2 and 9 (*Mmp2* and *Mmp9*), *Tgfβ*, *Vegfa* and hypoxia-inducible factor 1 alpha (*Hif1a)* were restored in CPT1AM-expressing mice (Fig. 6F). No changes were seen in the mRNA levels of *Col6a1* between the HFD groups (Fig. 6F). No changes in the iWAT local lipid profile were observed (Figs. S5C and D).

HFD-induced increases in *Leptin* mRNA levels were blunted in the HFD CPT1AM group (Fig. 6G). HFD tended to increase *Adiponectin* gene expression in the HFD GFP mice although this did not reach statistical significance. However, *Adiponectin* mRNA levels were reduced in the CPT1AM-implanted mice compared to the HFD GFP group (Fig. 6G). *Resistin* mRNA levels were lower in both HFD groups. However, the HFD CPT1AM group showed a tendency of restored levels (Fig. 6G). Interestingly, HFD-induced increases in iWAT *Cpt1a* mRNA levels were blunted in the HFD CPT1AM group (Fig. 6H). No changes were seen in other genes involved in lipid metabolism such as *Fas*, *Atgl*, *Plin1* and *Srebp1c* (data not shown). As expected, HFD reduced the gene expression of the mitochondrial complexes (CI, CIII, CIV and CV) (Fig. 6I). However, their expression was largely restored in the HFD CPT1AM group (Fig. 6I). The HFD CPT1AM group also showed restorations in the HFD-

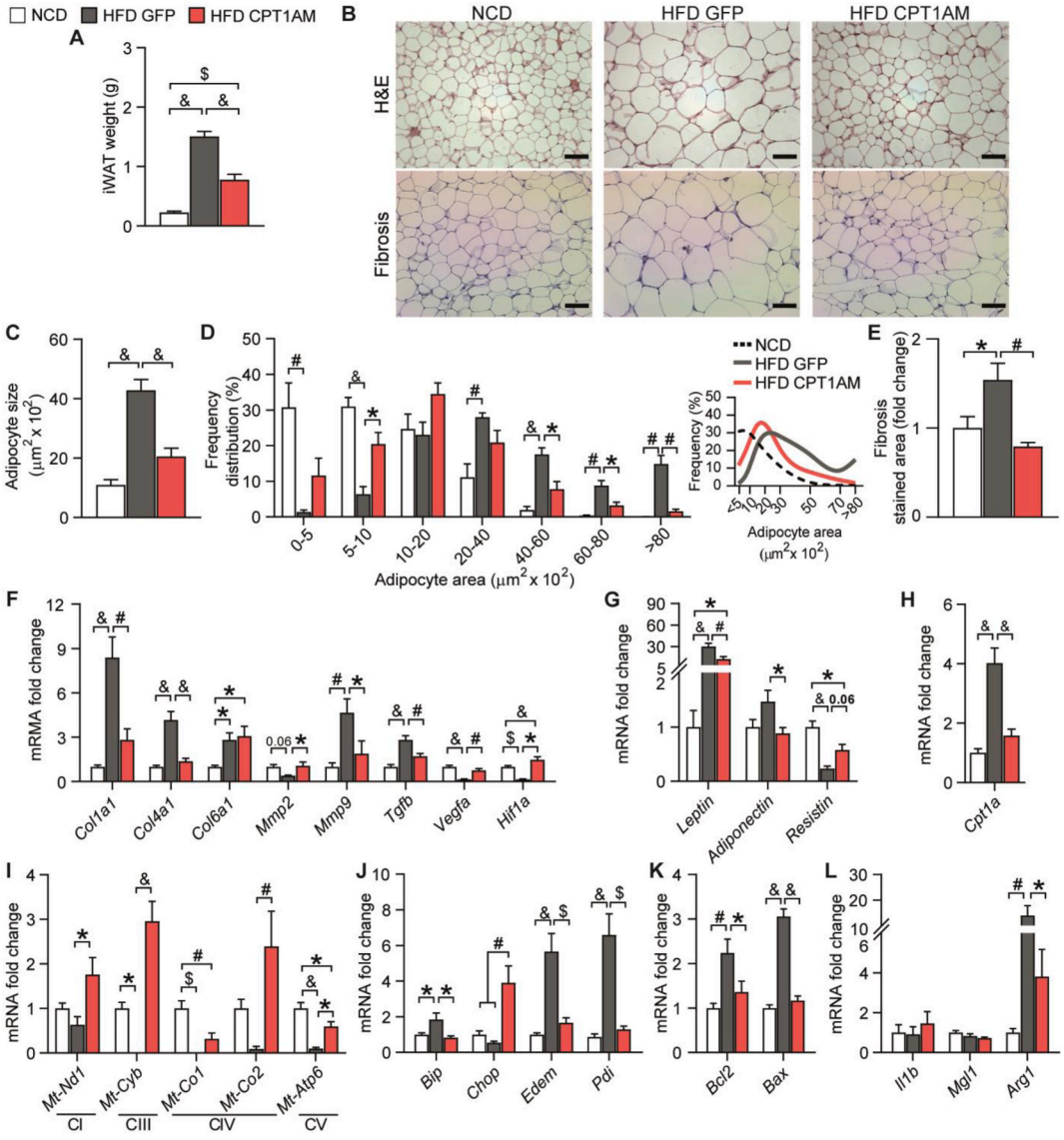

Fig. 6. CPT1AM-expressing adipocytes implantation prevented hypertrophy, fibrosis, mitochondrial dysfunction, ER stress and apoptosis in the iWAT of HFD-fed mice. (A) iWAT weight 10 weeks after the implantation. (B) Representative images of an iWAT section stained with H&E (top panels) and Masson's trichrome for fibrosis (bottom panels). Scale bar, 100 μm. Adipocyte size quantification (C) and morphometric analysis of the adipocyte frequency distribution (D). (E) Masson's trichrome quantification. mRNA levels of the genes associated with ECM remodeling (*Col1a1, Col4a1, Col6a1, Mmp2, Mmp9, Tgfb*, *Vegfa* and *Hif1a*) (F); the hormones secreted by AT (*Leptin*, *Adiponectin* and *Resistin*) (G); lipid metabolism (*Cpt1a*) (H); mitochondrial complexes (*Mt-Nd1*, *Mt-Cyb*, *Mt-Co1*, *Mt-Co2* and *Mt-Atp6*) (I); ER stress (*Bip, Chop, Edem* and *Pdi*) (J); apoptosis (*Bcl2* and *Bax*) (K) and inflammation (*Il1b*, *Mgl1* and *Arg1*) (L). Data are expressed as the mean ± SEM (n = 6–7). *p < 0.05, #p < 0.01, $p < 0.001, &p < 0.0001.

induced alterations of several genes involved in oxidative damage (*Bip*, *Edem* and *Pdi*; Fig. 6J) and apoptosis (B-cell lymphoma-2 (*Bcl2*) and Bcl2-associated X (*Bax*); Fig. 6K). Implantation of CPT1AM-expressing adipocytes lowered the HFD-induced increase in the expression of the M2 (alternative activation)-associated gene, *Arg1*, while no changes were seen in the expression of other inflammatory cytokines such as *Il1b* and *Mgl1* (Fig. 6L).

2.6. CPT1AM-implanted mice showed a reduction in HFD-induced gWAT hypertrophy, fibrosis, ER stress, apoptosis and inflammation, and improvements in leptin levels and lipid metabolism

Similar to that observed in the iWAT, HFD CPT1AM mice showed a reduction in gWAT mass (Fig. 7A), adipocyte size (Fig. 7B top panels, C and D) and fibrosis (Fig. 7B bottom panels, E). HFD-induced alterations in the mRNA levels of genes involved in ECM remodeling, fibrosis, and hypoxia (*Col1a1*, *Col4a1*, *Tgfb, Vegfa* and *Hif1a*) were reverted in the HFD CPT1AM group, without changes in *Col6a1*, *Mmp2* and *Mmp9* (Fig. 7F). No changes in the gWAT local lipid profile were observed (Figs. S5E and F). HFD-induced increases in *Leptin* expression were blunted in the HFD CPT1AM group (Fig. 7G). No differences between the HFD GFP and HFD CPT1AM groups were seen in *Adiponectin* and *Resistin* gene expression (Fig. 7G). While no changes were seen in *Glut4* mRNA levels, HFD-induced changes in *Hsl* and *Cpt1a* were blocked in the HFD CPT1AM group (Fig. 7H). Similar to that found in the iWAT, HFD-induced increases in the mRNA levels of genes involved in ER stress (*Edem* and *Pdi*) and apoptosis (*Bcl2* and *Bax*) were blunted in the HFD CPT1AM group (Fig. 7I and J). CPT1AM-implanted mice also showed a reduction in the HFD-induced increase in the mRNA levels of some anti-inflammatory genes such as *Il10* and *Arg1* (Fig. 7K). A trend was also seen for the inflammatory cytokine *Il1b* (Fig. 7K).

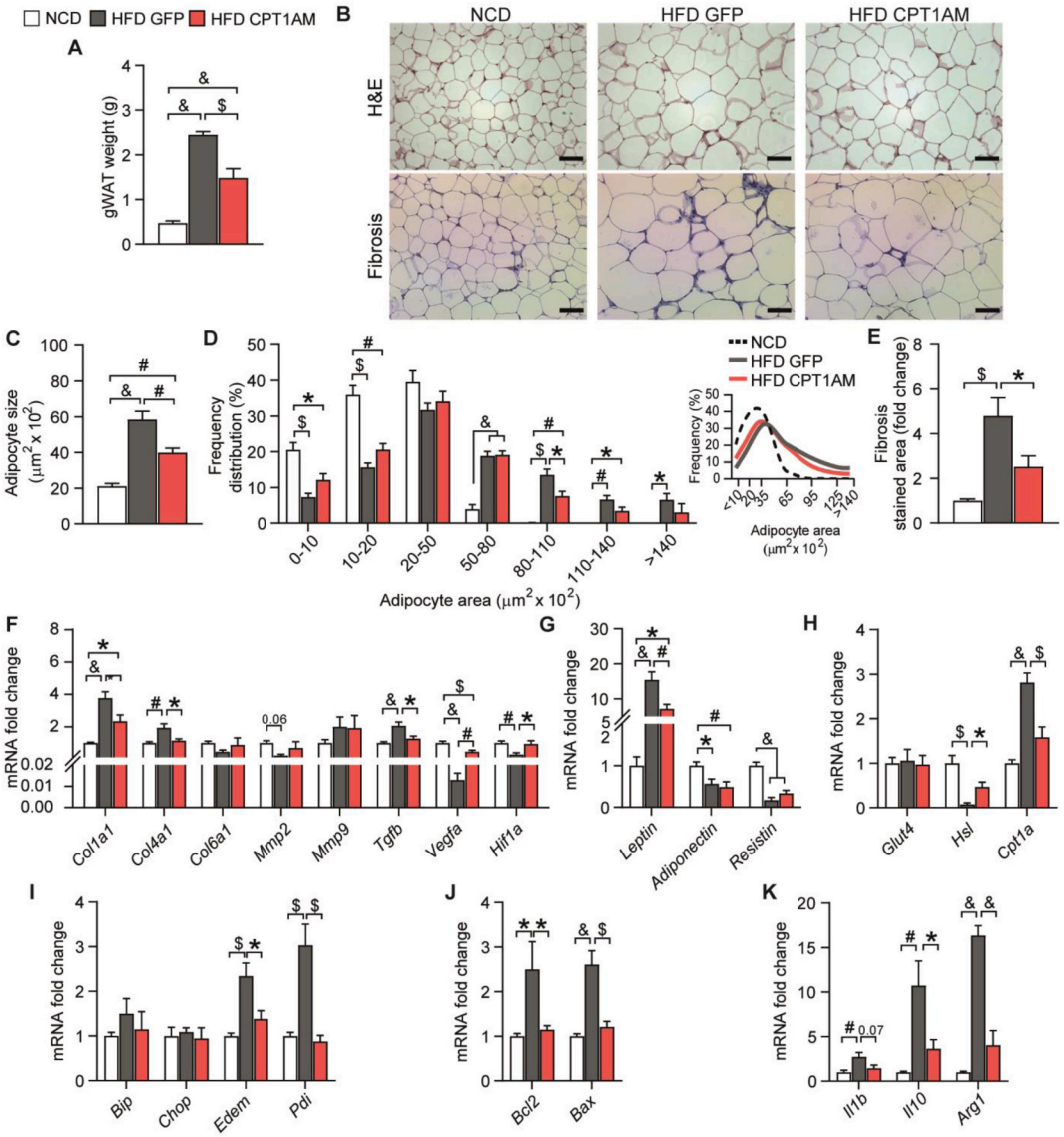

Fig. 7. CPT1AM-expressing adipocytes implantation reduced hypertrophy, fibrosis, ER stress, apoptosis and inflammation and improved leptin levels and lipid metabolism in the gWAT of HFD-fed mice. (A) gWAT weight 10 weeks after the implantation. (B) Representative images of a gWAT section stained with H&E (top panels) and Masson's trichrome for fibrosis (bottom panels). Scale bar, 100 μm. Adipocyte size quantification (C) and morphometric analysis of the adipocyte frequency distribution (D). (E) Masson's trichrome quantification. mRNA levels of the genes associated with ECM remodeling (*Col1a1, Col4a1, Col6a1, Mmp2, Mmp9, Tgfb*, *Vegfa* and *Hif1a*) (F); the hormones secreted by AT (*Leptin*, *Adiponectin* and *Resistin*) (G); glucose and lipid metabolism (*Glut4*, *Hsl* and *Cpt1a*) (H); ER stress (*Bip, Chop, Edem* and *Pdi*) (I); apoptosis (*Bcl2* and *Bax*) (J) and inflammation (*Il1b*, *Il10* and *Arg1*) (K). Data are expressed as the mean ± SEM (n = 6–7). *p < 0.05, #p < 0.01, $p < 0.001, &p < 0.0001.

2.7. HFD-induced alterations in thermogenesis, ECM remodeling, mitochondrial respiration, ER stress, apoptosis and inflammation were reverted in the iBAT of CPT1AM-implanted mice

The HFD CPT1AM group showed a reduction in the iBAT weight compared to HFD GFP controls (NCD: 0.075 g ± 0.005; HFD GFP: 0.108 g ± 0.009; HFD CPT1AM: 0.084 g ± 0.004; Fig. 8A). Accordingly, histological analysis indicated a decrease in the HFD-induced brown-to-white transformation in the HFD CPT1AM group (Fig. 8B). The analysis of the iBAT local lipid profile indicated that HFD-induced increase in TGs showed a tendency to be reduced in CPT1AM-expressing mice (Fig. S5G). No changes were observed in free cholesterol levels (Fig. S5H).

HFD-induced increases in the mRNA levels of the thermogenic genes *Ucp1*, *Prdm16* and *Pparg* were blunted in the CPT1AM-implanted mice (Fig. 8C). No changes were observed in other thermogenic genes such as *Pgc1a*, *Bmp8p* and cell death-inducing DNA fragmentation factor alpha-like effector A (*Cidea*) (Fig. 8C). The iBAT from CPT1AM-implanted mice showed reversals of the HFD-induced alterations in the mRNA levels of genes involved in ECM remodeling and hypoxia (*Col4a1*, *Tgfb, Vegfa* and *Hif1a*), mitochondrial complexes (CI, CIII, CIV and CV), ER stress (*Bip, Edem* and *Pdi*), apoptosis (*Bcl2* and *Bax*) and inflammation (*Il1b, Il10* and *Arg1*) (Fig. 8D–H). Next, we analyzed the iBAT mRNA levels of genes involved in glucose and lipid metabolism (Fig. 8I). No changes were seen in the expression levels of *Glut4*, *Atgl* and *Cpt1b*. *Hsl* and *Fas* mRNA levels were decreased in the HFD GFP mice compared to the NCD control. However, only *Hsl* gene expression was restored in the HFD CPT1AM group (Fig. 8I).

3. Discussion

Despite the titanic efforts of social, government and research

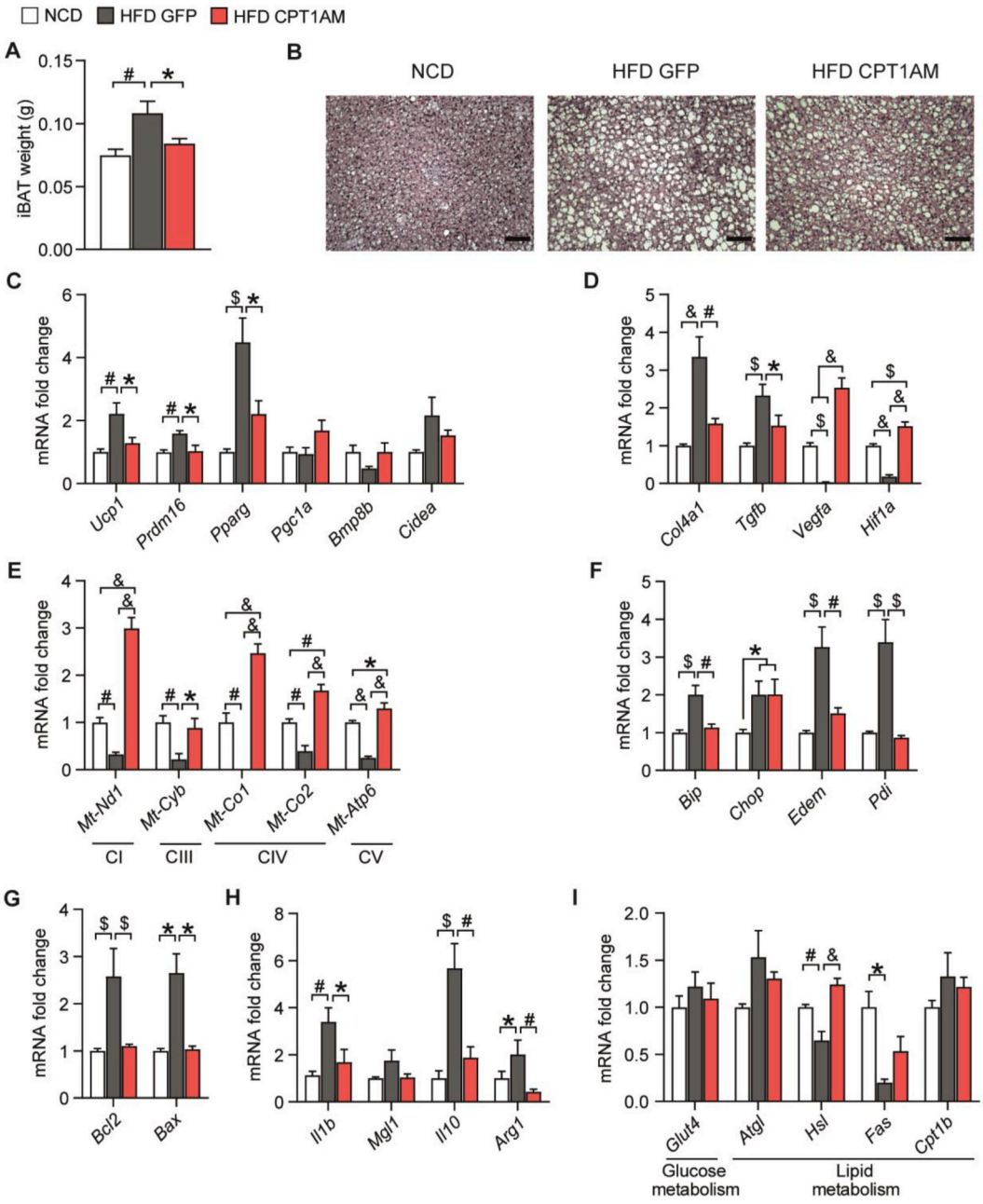

Fig. 8. Implantation of AT-MSC-derived adipocytes expressing CPT1AM restored HFD-induced alterations in thermogenesis, ECM remodeling, mitochondrial dysfunction, ER stress, apoptosis and inflammation in the iBAT of HFD-fed mice. (A) iBAT weight 10 weeks after the implantation. (B) Representative image of an iBAT section stained with H&E. Scale bar, 100 μm. mRNA levels of the genes associated with thermogenesis (*Ucp1, Prdm16, Pparg, Pgc1a, Bmp8b* and *Cidea*) (C); ECM remodeling (*Col4a1, Tgfb, Vegfa* and *Hif1a*) (D); mitochondrial complexes (*Mt-Nd1, Mt-Cyb, Mt-Co1, Mt-Co2* and *Mt-Atp6*) (E); glucose and lipid metabolism (*Glut4, Atgl, Hsl, Plin1, Plin5, Fas, Srebp1c* and *Cpt1b*) (F); ER stress (*Bip, Chop, Edem* and *Pdi*) (G); apoptosis (*Bcl2* and *Bax*) (H) and inflammation (*Il1b, Mgl1, Il10* and *Arg1)* (I). Data are expressed as the mean ± SEM (n = 6–7). *p < 0.05, #p < 0.01, $p < 0.001, &p < 0.0001.

communities, the global epidemic of obesity continues to rise and novel therapeutic approaches are urgently needed. MSCs have gained great interest for their clinical application in cell therapy. An excessive accumulation of fat and a low utilization of lipids are one of the main drivers of obesity. Increasing amounts of evidence indicate that enhanced lipid metabolism through CPT1AM expression is a good strategy for reducing excessive lipids (Serra et al., 2013; Orellana-Gavaldà et al., 2011; Weber et al., 2020). In this study we designed for the first time a new approach that involves an *ex vivo* implantation of AT-MSC-derived adipocytes expressing CPT1AM to ameliorate obesity and diabetes. The choice of CPT1AM was based on the following points: (1) the CPT1A isoform has a lower sensitivity to malonyl-CoA inhibition and a higher affinity for the carnitine substrate than CPT1B (McGarry et al., 1983) and (2) the permanently active mutant CPT1AM ensures constantly high levels of FAO, independently of malonyl-CoA levels (Herrero et al., 2005b). The latter point is particularly relevant in obesity, where in addition to high lipid levels, high glucose levels (and, therefore, high malonyl-CoA levels) also occur.

We demonstrated that AT-MSCs can be isolated from different fat depots (iWAT, gWAT and BAT) in young or adult and lean or obese and hyperglycemic mice and cultured *in vitro*. In our hands, all isolated AT-MSCs exhibited the specific characteristics of MSCs (Dominici et al., 2006). First, they were able to be maintained as adherent cells in culture and exhibited a fibroblastic-like morphology. Second, they

differentiated into three different lineages (adipocytes, osteocytes and chondrocytes), demonstrating their multipotentiality. Finally, isolated AT-MSCs expressed specific surface markers (CD90, CD105, CD29 and Sca1) and did not express the hematopoietic markers CD34 and CD45. In accordance with the findings in the literature, (Cannon and Nedergaard, 2004; Ussar et al., 2014; Petrovic et al., 2010; Seale et al., 2007) gWAT- or iWAT-isolated AT-MSC-derived beige adipocytes expressed *Tmem26*, while iBAT-isolated AT-MSC-derived brown adipocytes showed high expression of the specific brown adipocyte markers *Zic1* and *Ucp1*. Unlike iWAT, gWAT-isolated AT-MSC-derived beige adipocytes did not express the thermogenic marker *Ucp1* until they were induced with a β-adrenergic stimulus. This is consistent with the intrinsic differences between the two fat depots, where beige adipocytes are more abundant in iWAT than in gWAT (Zhang et al., 2018; Vitali et al., 2012; Zuriaga et al., 2017; Nahmgoong et al., 2022).

Several studies have demonstrated that the transplantation of MSCs, MSC-derived exosomes, BAT or beige/brown adipocytes can reduce body weight in obese mice (Soler-Vázquez et al., 2018; Calvo et al., 2021; Cai et al., 2022; White et al., 2019; Payab et al., 2020; Lu et al., 2020; Zhao et al., 2018). However, the effectiveness of beige/brown adipocyte transplantation may depend on several factors such as the source and number of transplanted cells, the microenvironment of the recipient site (*i.e.*, the location of the transplant), the type of thermogenic activator used to promote adipocyte browning and the duration of the transplantation. All of these might influence the maintenance of the beneficial effects of the transplantation over longer periods of time. Based on these studies, we tested whether the adipocytes infected with the LV-GFP control *per se* improved the obese and diabetic phenotype. We did not find changes in body weight, food intake, glucose levels or glucose tolerance between the two control groups (HFD MG and HFD GFP) 10 weeks after implantation (Fig. S4). Our results indicated that the total amount of implanted adipocytes (10 (Mushahary et al., 2017) cells/mouse) was not sufficient to induce a phenotypic or metabolic change in the HFD GFP mice. Of note, in our experiments, cells were not incubated with a thermogenic activator such as PRDM16 (Kishida et al., 2015) or Forskolin (Min et al., 2016). Moreover, we used a lower number of cells (10 times lower) compared with other studies, while the duration of the experiment was similar (Min et al., 2016).

iWAT-isolated AT-MSC-derived adipocytes were able to be infected with lentivirus carrying the CPT1AM gene, which led to an increase in CPT1A protein levels, CPT1 activity and FAO. The lentivirus vectors were chosen for their ability to infect non-dividing cells such as mature adipocytes, their integration into the cell genome, their duration, and their low immunogenicity. Five weeks after the HFD treatment, CPT1AM-implanted mice showed a lower body weight compared to their HFD GFP control littermates. This was consistent with other studies where transplantations were performed with *Prdm16*-, *C/ebp-b*- and *L-myc*-expressing brown adipocytes (Kishida et al., 2015). Moreover, 6-week-old mouse BAT transplantation into *ob/ob* mice (Liu et al., 2015) or HFD-induced obese mice (Zhu et al., 2014; Liu et al., 2013) promoted a similar decrease in body weight. Consistent with other studies, (Liu et al., 2015; Zhu et al., 2014; Stanford et al., 2013; Shankar et al., 2019) we did not see changes in food intake between the HFD GFP and HFD CPT1AM groups.

Importantly, CPT1AM-implanted mice showed a reversal of the HFD-induced increases in blood glucose, insulin and leptin levels and glucose intolerance. Other studies report an improvement in glucose and insulin metabolism after the transplantation of thermogenic adipocytes or BAT (Silva et al., 2014; Kishida et al., 2015; Chen et al., 2018; Liu et al., 2013, 2015; Zhu et al., 2014; Stanford et al., 2013; Shankar et al., 2019; Wu et al., 2017; Yuan et al., 2016; Oguri et al., 2017; Kikai et al., 2017). However, we observed that CPT1AM-implanted mice also showed lower circulating cholesterol, HDL cholesterol and glycerol levels. HDL cholesterol levels are mainly the reflection of the liver lipid status. *I.e.* Higher hepatic levels concomitant with the upregulation of lipogenic genes in HFD-fed mice indicate higher HDL (and VLDL) synthesis. Thus, the restoration in lipoproteins and glycerol levels in the CPT1AM-expressing mice might indicate a restoration of the VLDL flux from the liver and lipolysis, respectively. We could not disregard a potential contribution of the adipose tissue in these pathways. No changes were seen in other lipid and lipoproteins with a higher turnover such as TGs or VLDL and LDL. It is relevant to highlight that the subcutaneously implanted iWAT-isolated AT-MSC-derived adipocytes were still present in the dorsal area of the mice 10 weeks after the implantation. At this time point, the implanted CPT1AM-expressing adipocytes showed increased expression of *Cpt1a* and two thermogenic genes such as *Pgc1a* and *Prdm16* (the transcription factor involved in brown adipocyte differentiation), compared to the implanted control GFP-expressing adipocytes. Consistently with our data, Spiegelman and colleagues have linked transgenic expression of *Prdm16* in WAT with improved glucose tolerance and reduced weight gain in HFD-fed mice (Seale et al., 2011). Recently, Rojas-Rodriguez et al. reported that primed adipose progenitor cell-differentiated adipocytes formed structured AT *in vivo* 16 weeks after transplantation (Rojas-Rodriguez et al., 2019). Other studies also show functional and viable adipocytes after several time periods post-transplantation (Silva et al., 2014; Kishida et al., 2015). Consistent with these studies, no differences were observed between the GFP and CPT1AM-expressing implants in terms of apoptosis (Caspase 3 staining) nor macrophages and T cells infiltration. Since implanted cells were embedded in a matrigel matrix and grafted subcutaneously we expect low probability of cell migration. In fact, CPT1AM-specific mRNA levels in other tissues such as liver, gWAT, iWAT and BAT were undetectable (data not shown).

To evaluate the impact of CPT1AM-expressing AT-MSC-derived adipocyte implantation on obesity, we analyzed the major peripheral tissues involved in its pathophysiology: the liver, iWAT, gWAT and iBAT. CPT1AM-implanted mice showed a reduction in the HFD-induced increase in hepatic steatosis (measured as liver TG content). Hepatic steatosis is mainly caused by an imbalance between liver lipolysis and *de novo* lipogenesis. Consistently, CPT1AM-implanted mice showed a reversal of the HFD-induced alterations in the expression of lipolytic (*Hsl*) and lipogenic (*Acc1, Scd1* and *Dgat1*) genes. HSL is the rate-limiting lipolytic enzyme in TG hydrolysis and its deficiency increases the accumulation of toxic lipids such as DAGs in hepatocytes, promoting lipotoxicity (Haemmerle et al., 2002). Insulin inhibits the lipolytic activity of HSL (Calderon-Dominguez et al., 2016a). Thus, we hypothesize that the lower circulating insulin levels in CPT1AM-implanted mice might enhance and restore the liver lipolytic gene expression levels. *Ucp2* mRNA levels were increased in HFD-treated CPT1AM-implanted mice, most likely to reduce HFD-induced increases in hepatic ROS levels. Importantly, CPT1AM-implanted mice on an HFD also showed reduced hepatic oxidative stress and improved lipid, glucose, and cholesterol metabolism.

HFD-induced increases in iWAT and gWAT hypertrophy, fibrosis, ER stress, apoptosis and inflammation were reduced in the CPT1AM-implanted mice. In addition, the expression of the mitochondrial complexes was improved in the iWAT of CPT1AM-implanted mice. In obesity, AT suffers from hypoxia and undergoes strong ECM remodeling, generating fibrotic and damaged tissue. Fibrosis is largely generated by collagen deposition, the major component of the ECM (Lin et al., 2016). At the transcriptomic level, it has been shown that these alterations begin after 8 weeks of 60% HFD, although they become more evident with longer exposure to the diet (Jones et al., 2020; Alcalá et al., 2017). These alterations decrease tissue flexibility and contribute to AT dysfunction and inflammation. Importantly, both collagen deposition and *Col1a1, Col4a1*, *Tgfb*, *Vegfa* and *Hif1α* expression were restored in the iWAT, gWAT and iBAT of the HFD CPT1AM group. The expression and serum levels of hormones such as leptin were decreased in the WAT of the HFD CPT1AM group compared to the HFD GFP group, most likely contributing to the improvement in the peripheral phenotype.

The weight of iBAT was reduced in the HFD CPT1AM group compared to the HFD GFP controls. This indicated a reduction in the

brown-to-white transformation histologically seen in obesity. Consistently, HFD-induced alterations in the mRNA levels of genes involved in ECM remodeling, mitochondrial respiration, ER stress, apoptosis and inflammation were restored in the iBAT of CPT1AM-implanted mice. Importantly, HFD-induced increases in the mRNA levels of the thermogenic genes *Ucp1*, *Prdm16* and *Pparg* were reversed in the CPT1AM-implanted mice. This pointed towards a general improvement in the thermogenic capacity of the HFD CPT1AM mice. As observed in the liver and gWAT, the expression levels of *Hsl* were also restored in the iBAT of CPT1AM-implanted mice.

Altogether, we hypothesize that the enhanced FAO rate of the CPT1AM-implanted adipocytes might have drained the HFD-induced excess of lipids in peripheral tissues, reducing liver steatosis and adipose tissue weight, improving lipid and carbohydrate metabolism and leading to a decrease in the circulating insulin and leptin levels. We cannot rule out the possibility that other circulating factors and/or alternative mechanisms could drive the reduced lipid overload and improved phenotype. Recent studies have shown that AT secretes signaling protein-containing extracellular vesicles that can integrate into other tissues (Crewe and Scherer, 2022; Camino et al., 2020). This highlights other possibilities of crosstalk between the implanted AT and the improvement in the peripheral phenotype.

Before the gene and cell therapy approach presented here can be translated into a viable therapy against human obesity, several considerations must be considered. First, although we were able to isolate mouse MSCs from iWAT, gWAT and iBAT, when performing a surgical resection in humans such as liposuction or bariatric surgery, the scWAT is more accessible and its dissection less invasive than that of the visceral WAT or BAT. Thus, scWAT would be the depot of choice. Second, several studies have correlated impaired AT-MSC function with age, cell senescence, apoptosis, autophagy, ROS and mitochondrial dysfunction (Conley et al., 2020; Cramer et al., 2010; Duscher et al., 2014). Aging, obesity and metabolic dysfunction promote the senescent state of these cells, *i.e.*, modifying their typical fibroblastic morphology to a flattened polygonal shape (Hass et al., 2011; Liu et al., 2017). Importantly, a greater number of senescent cells leads to a lower differentiation efficiency (Mastrolia et al., 2019; Hass et al., 2011; Conley et al., 2020; Liu et al., 2017; Kornicka et al., 2018; Hristov et al., 2019; Fijany et al., 2019; Barbagallo et al., 2017; Rennert et al., 2014). Thus, in a potential future application of this approach in humans, the age and metabolic status of the donor and the senescent status of the isolated AT-MSCs should be carefully evaluated. Riis et al. describe some critical steps in the process of isolating and expanding AT-MSCs (Riis et al., 2015). These involve several factors including the AT source, age, the metabolic state of the donor, the enzymatic or non-enzymatic method of isolation, the culture medium and even the seeding density. Here, we optimized the number of passages, cell confluence and the size of the well where the cells were seeded, since these factors can affect MSC senescence (Legzdina et al., 2016; Neuhuber et al., 2009). Thus, we were able to isolate, characterize and differentiate AT-MSCs from different fat depots, independently of the age and metabolic state of the mice. However, to avoid any potential interference of these important factors, we proceeded with the implantation of iWAT-isolated AT-MSC-derived adipocytes from healthy and lean adult mice donors. Third, although the source and isolation method of the MSCs could be similar in rodents and humans, there might be differences in the duration and capacity for differentiation into adipocytes as well as the outcome obtained. Finally, our studies analyzed transplantation over a short-term period. Long-term studies would have to carefully analyze whether (1) the implant is still viable and functional, (2) the improvement in the obese phenotype is maintained, and (3) compensatory mechanisms, such as increased food intake, can overcome its metabolic benefit.

In summary, our results reveal that iWAT-, gWAT- or iBAT-derived MSCs from young healthy adult or obese and hyperglycemic mice exhibit MSC-specific characteristics. In addition, the implantation of CPT1AM-expressing AT-MSC-derived adipocytes into HFD-fed mice reduces obesity and hyperglycemia, including body weight gain, glucose intolerance, and serum insulin, leptin, HDL and total cholesterol and glycerol levels, while also improving the obese phenotype in peripheral tissues, including lipid accumulation, and cellular stress, apoptosis and inflammation at the mRNA levels. From a clinical perspective, the most important potential application of this study is the finding that in humans, AT-MSCs can be isolated from samples obtained during liposuction or bariatric surgery that can then undergo gene therapy modification and implantation into the same individual to improve the obese phenotype. This autologous transplantation highlights a potential personalized medicine approach with minor immunological responses.

4. Material & methods

4.1. Animals

Seven-week-old male C57BL/6J mice were purchased from Janvier Labs, France, and housed in an animal facility for 1 week to acclimatize prior to the experiments. Eight-week-old mice were divided into two groups and fed either an NCD (10% kcal from fat derived mainly from saturated (2.7%), monounsaturated (3.1%) and polyunsaturated (3.8%) fatty acids, 18% kcal from proteins and 72% kcal from carbohydrates, 3.76 kcal/g. International Products Supplies Limited, TestDiet, UK, 58Y2) or a 60% HFD (62% kcal from fat derived mainly from saturated (23.9%) and monounsaturated fatty acids (24.4%), 18% kcal from proteins, 20% kcal from carbohydrates, 5.1 kcal/g. International Products Supplies Limited, TestDiet, 58Y1) to induce obesity. Animals were maintained at 22 ± 2 °C and 50–60% humidity, with a 12-h light/dark cycle and *ad-libitum* access to food and water. Animals were fasted overnight, anesthetized with 4% isoflurane and sacrificed by cervical dislocation. All the procedures with mice were approved by the Animal Experimentation Ethics Committee of the University of Barcelona (CEEA-UB), with procedure number CEEA 10190, 140/18 P4 obtained from the Government of Catalonia.

4.2. AT-MSC isolation and culture

Young mice (3–4 weeks old), adult mice (8 weeks old) or HFD-induced obese animals (16–20 weeks old) were sacrificed by cervical dislocation for subsequent AT excision. Fat depots were placed in DMEM/F12 (Gibco™, Germany, 11594426) containing 1.5% penicillin/streptomycin (P/S) (Gibco™, 15140122). Tissues were washed twice with DMEM/F12, minced and digested with a collagenase digestion solution [100 mM HEPES, pH 7.4, 123 mM NaCl, 5 mM KCl, 3 mM $CaCl_2{\cdot}2H_2O$, 5 mM glucose, 1.5% fatty acid-free bovine serum albumin and 1 mg/ml of type I collagenase (Worthington Biochemical Products, NJ, USA, LS004196)] at 37 °C for 45 min. Type I collagenase activity was inactivated by adding DMEM/F12 supplemented with 10% heat-inactivated fetal bovine serum (HI-FBS) (Gibco™, 10270106). The solution was filtered through a sterile 250-μm mesh (Vidra Foc, Spain, FMNY250125) and recovered bottom-up with a 19-gauge needle to pass through a 70-μm cell strainer (Corning, NY, USA, 431751). The stromal vascular fraction was obtained by centrifugation at 2300 rpm for 10 min. The pellet was resuspended in red blood lysis buffer (155 mM NH_4Cl, 10 mM K_2CO_3 and 0.1 mM EDTA) for 10 min. The cells were washed with DMEM/F12 containing 1% P/S and centrifuged at 2300 rpm for 8 min. The pellet was resuspended in complete medium (CM) [DMEM/F12 supplemented with 10% HI-FBS and 1% P/S] and plated onto 6-well plates. The next day, the cells were washed twice with DPBS, pH 7.4 (Sigma-Aldrich, MA, USA, D1408), before CM was added again. At 90% confluency, AT-MSCs were harvested with 0.05% trypsin/EDTA (Gibco™, 25300–062) and seeded at a density between 10,000 and 20,000 cells/cm^2. Experiments were typically performed at passage 3–5. AT-MSC primary cultures were maintained in a humidified incubator at 37 °C and 5% CO_2.

4.3. Induction of AT-MSCs into multilineage differentiation

4.3.1. AT-MSC differentiation into brown adipocytes

AT-MSCs from iBAT began to differentiate at 50–60% confluence, as previously described (Calderon-Dominguez et al., 2016b). CM was replaced with the brown adipocyte differentiation medium (Brown-DM) [CM supplemented with 20 nM insulin (Sigma-Aldrich, I0516) and 1 nM triiodothyronine (T3) (Sigma-Aldrich, T6397)]. On the next day (day 0), cells were incubated with brown adipocyte induction medium (Brown-IM) [CM containing 0.5 μM dexamethasone (Sigma-Aldrich, D6645), 1 μM rosiglitazone (Sigma-Aldrich, R2408), 0.125 μM indomethacin (Sigma-Aldrich, I7378) and 0.5 mM isobutyl methylxanthine (IBMX) (Sigma-Aldrich, I7018)]. Brown-IM was replaced after 40 h with Brown-DM on day 2 of differentiation until complete differentiation. Experiments with brown adipocytes were performed on day 6 of differentiation.

4.3.2. AT-MSC differentiation into beige adipocytes

When AT-MSCs from gWAT or iWAT were at 80–90% confluence, the beige adipocyte induction medium (Beige-IM) [CM supplemented with 5 μg/ml of insulin, 10 nM T3, 1 μM dexamethasone and 500 μM IBMX] was added. After 72 h (day 0), cells were incubated with beige adipocyte differentiation medium (Beige-DM) [CM containing 5 μg/ml of insulin and 1 μM rosiglitazone] for 12 days until complete adipocyte differentiation. In some experiments, cells were stimulated with a thermogenic β-adrenergic agonist, 5 μg/ml (v/v) of CL-316,243 (Sigma-Aldrich, C5976), for 4 h before cell harvest.

4.3.3. Osteogenic differentiation

AT-MSCs were cultured until 80–90% confluence. On day 0, osteoblast differentiation medium [CM supplemented with 0.01 μM dexamethasone, 10 mM β-glycerophosphate (Sigma-Aldrich, G6251) and 50 μg/ml of ascorbate-2-phosphate (Sigma-Aldrich, A8960)] was added until differentiation was complete on day 21. The differentiation into osteoblasts was observed by Alizarin Red S staining, which forms complexes in a chelation process with extracellular calcium deposits produced by these cells, resulting in a bright red stain. On day 21 of differentiation, the cells were rinsed twice with DPBS, fixed with 4% (w/v) paraformaldehyde (PFA) for at least 10 min and washed twice with distilled H_2O. After two washes, 2% (w/v) Alizarin Red S solution (pH 4.1–4.3) (Sigma-Aldrich, A5533) was added and incubated for 15 min at 100 rpm. After two washes in distilled water, 4% PFA was added and the cells were ready for observation by bright field microscopy.

4.3.4. Chondrogenic differentiation

5×10^5 AT-MSCs were seeded into a conical tube, where they were centrifuged for 5 min at 500 *g* to form a pellet. Chondrocyte differentiation medium [DMEM (Gibco™, 21885108) containing 20% HI-FBS, 1% P/S, 30 mM HEPES, 1 ng/ml of basic FGF (Sigma-Aldrich, F0291) and 5 ng/ml of TGF-β1 (Sigma-Aldrich, H8541)] was added for 4 weeks. After the differentiation process, pellets were fixed in 10% formalin solution (Sigma-Aldrich, HT5017) for 24 h. Samples were embedded in paraffin and cut into 5-μm sections. After deparaffinization and hydration with dH2O, sections were stained with toluidine blue (Sigma-Aldrich, 198161) solution [1% toluidine blue (w/v) and 1% sodium chloride (w/v) (1:10), pH 2.0–2.5] for 2–3 min, which has a high affinity for the sulfate groups in the proteoglycans produced by chondrocytes. Sections were washed 3 times with dH_2O, dehydrated with 95% and 100% ethanol, and cleared in a xylene substitute. Chondrocytes were observed by bright field microscopy.

4.4. Oil Red O staining

The fatty acid storage capacity of the differentiated adipocytes was determined by observing the accumulation of neutral TGs and lipids inside lipid droplets. Oil Red O staining allows them to be stained and identified through their bright red color. Cells were washed twice with DPBS and fixed with 4% (w/v) PFA for 30 min. The cells were then rinsed twice in distilled H_2O, incubated with 60% isopropanol for 5 min and stained with filtered Oil Red O (Sigma-Aldrich, O0625) solution [0.3% (w/v) Oil Red O:H_2O (3:2)] for 15 min. Cells were washed several times with dH_2O and visualized under a microscope. Furthermore, for the quantification of the amount of accumulated neutral lipids, cells were left to dry for 10 min and incubated with 100% isopropanol for 10 min on ice, before the optical density (OD) was determined at a wavelength of 492 nm.

4.5. Flow cytometry

AT-MSCs were harvested, washed and resuspended at 2×10^6 cells/ml in DPBS containing 2% HI-FBS. Then, 2×10^5 cells were incubated with the specific antibodies or isotype control antibodies on ice for 45 min. The antibodies used were against: CD29 (0.5 μg, 11.0291–82; isotype control, 11-4888-81), CD34 (1 μg, 56-0341-82; isotype control, 56-4321-80), CD45 (0.5 μg, 69-0451-82; isotype control, 69-4031-80), CD90 (0.06 μg, 12-0902-81; isotype control, 12-4321-80), CD105 (0.125 μg, 17-1051-82; isotype control, 17-4321-81) and Sca1 (0.25 μg, 63-5981-80; isotype control, 63-4321-80). All these antibodies were from eBioscience™, CA, USA. After the incubation time, all samples were washed in DPBS containing 2% HI-FBS and centrifuged for 5 min at 300 *g*. AT-MSCs were analyzed using a Gallios flow cytometer and the FlowJo software (v10.0.7r2, LLC).

4.6. Lentiviral vectors

The CPT1AM-IRES2-GFP fragment from the pTRE3G-CPT1AM-IRES2-GFP vector (the group of Serra and Herrero, University of Barcelona, Spain) was amplified by PCR using Phusion™ High–Fidelity DNA Polymerase (Thermo Scientific, MA, USA, F530S) with the forward primer 5′-CTCCCCAGGGGGATCCATGGCAGAGGCTCACCAAG-3′ and the reverse primer 5′-GAGGTTGATTGTCGACTTACTTGTACAGCTCGTCCATGC-3'. Then, the CPT1AM-IRES2-GFP fragment was cloned into a *Bam*HI- *Sal*I-digested pCCL-hPGK-dNGFR-IRES-GFP-Wpre vector (kindly provided by Dr. Antonia Follenzi, Università del Piemonte Orientale, Scuola di Medicina, Novara, Italy) using the In-Fusion Cloning Kit and One Shot® TOP10 Chemically Competent *E. coli* (Invitrogen™, MA, USA, C404010), following the manufacturer's instructions. The resulting lentiviral vector was pCCL-hPGK-CPT1AM-IRES2-GFP-Wpre. To obtain vesicular stomatitis virus (VSV)-pseudotyped lentiviral stocks, we cotransfected pCCL-hPGK-CPT1AM-IRES2-GFP-Wpre or the corresponding GFP control transfer constructs, the third-generation packaging constructs pMDLg/pRRE and pRSV-REV, and the pMD2. G envelope into 293T cells, followed by ultracentrifugation of medium, as described (Follenzi et al., 2002). Titering of the vector on HEK 293T showed 2 to 6 $\times$ 10^8 TU/ml for the pCCL-hPGK-CPT1AM-IRES2-GFP-Wpre and 4,6 $\times$ 109 TU/ml for the GFP control.

4.7. LV transduction of AT-MSCs

On day 6 of differentiation, AT-MSC-derived adipocytes were incubated with concentrated lentivirus for 72h in Beige-DM (half of the volume recommended for the corresponding vessel size) supplemented with 5 μg/ml of polybrene, resulting in 10 MOI (multiplicity of infection). The next day, the same amount of fresh Beige-DM was added. Mdium was replaced with Beige-DM on day 9 of differentiation until complete differentiation of the adipocytes on day 12.

4.8. Implantation

At 8 weeks of age, 25 animals were randomly assigned to receive Matrigel (control group, MG), AT-MSC-derived adipocytes that

expressed the LV-GFP control (control group, GFP) or LV-CPT1AM (treated group, CPT1AM), as well as an NCD or HFD. The next day, infected adipocytes, in a total of 18 dishes (9 dishes per condition), were washed with DPBS and harvested with 0.05% Trypsin-EDTA. After centrifugation, 10^6 cells were suspended in Matrigel (Corning, 356231) (1:2) at a final volume of 300 μl. Recipient male mice were anesthetized with 2.5% isoflurane inhalation and the cells were injected into the back in the dorsal region and below the interscapular area with an 18-gauge needle.

4.9. Body weight and food intake measurements

In all the experiments, animals were weighed on a precision scale once a week throughout their lives. In addition, cumulative food intake was calculated as the difference between the added food and the food remaining the following week until the experiment was completed.

4.10. RNA extraction, cDNA synthesis and quantitative real-time PCR

Total RNA was extracted from cells or from non-fatty tissues using the Trizol reagent (Sigma-Aldrich, T9424). Tissues with a high lipid content such as iBAT, gWAT and iWAT were processed using the QIAzol lysis reagent from the RNeasy Lipid Tissue Mini Kit (QIAGEN, Germany, 74804), according to the manufacturer's protocol. For cDNA synthesis, the TaqMan Reverse Transcription Kit (Applied Biosystems, CA, USA, N8080234) was used. qRT-PCR was performed using a LightCycler® 480 Instrument II (Roche, Switzerland, 05015243001) and the SYBR Green PCR Master Mix Reagent Kit (Roche, 4887352001), following the manufacturer's instructions. All primer sequences are detailed in Table S1. The gene expression in liver, gWAT, iWAT, and iBAT was normalized to Ribosomal Protein L32 (RPL32). The instability of housekeeping in AT-MSCs during proliferation and differentiation has been described (Fink et al., 2008). Thus, in the case of the gene expression of AT-MSCs, the geometric mean of the TATA box-binding protein (TBP), the ribosomal RNA 18S (18S), the ribosomal protein L32 (RPL32) and the glyceraldehyde-3-phosphate dehydrogenase (GAPDH) was used for normalization.

4.11. Protein extraction and western blotting

Infected adipocytes were lysed with protein extraction buffer [30 mM HEPES, 150 mM NaCl, pH 7.4, 10% (v/v) glycerol, 1% (v/v) Triton X-100, 0.5% (w/v) sodium deoxycholate (DOC), a cOmplete Mini Protease Inhibitor Cocktail Tablet (Roche, 11836153001) and a PhosSTOP Phosphatase Inhibitor Tablet (Roche, 04906837001)]. Protein quantification was performed with the Pierce™ BCA Protein Assay Kit (Thermo Scientific™, 23225). The protein samples were separated on 10% acrylamide SDS-PAGE gels and transferred onto a 0.45-μm nitrocellulose membrane (Bio-Rad, 1620115). The antibodies used were: rabbit CPT1A-specific polyclonal primary antibody produced in our laboratory [Sci Crunch Cat# CPT1A, RRID:AB 2636894 (1:6000 in 5% milk in PBS-Tween)]; secondary goat anti-rabbit IgG, HRP-linked Ab [Santa Cruz, sc-2004 (1:10,000 in 5% milk in PBS-Tween)]; and mouse anti-β-actin-HRP [Sigma-Aldrich, A3854 (1:25,000 in 5% milk in PBS-Tween)].

4.12. Hepatic triglyceride determination

Liver TGs were extracted from 100 mg of tissue by adding 500 μl of 0.1% SDS. Tissue was homogenized and incubated overnight at room temperature under constant shaking. On the next day, 350 μl were used for TG extraction with methanol, chloroform and 0.5 M KCl. The extracted TGs were resuspended in 100% ethanol and quantified using the Serum Triglyceride Determination Kit (Sigma-Aldrich, TR0100-1 KT), according to the manufacturer's instructions.

4.13. Glucose levels and glucose tolerance test (GTT)

Four weeks post-implantation, glucose levels were measured from blood samples obtained from the tail vein after a 6h fast using a hand glucometer (Bayer, Contour XT, 83415194) and its test strips (Bayer, Contour Next, Germany, 84191389). The GTT was performed 9 weeks post-implantation after a 12h fast. For the GTT, 20% glucose (Baxter, IL, USA, 2B0124P) was administered intraperitoneally at a final dose of 2 g/kg body weight. Then, blood glucose was determined at 0, 15, 30, 60, 90 and 120 min after the injection.

4.14. Serum determinations

Blood samples were collected after 12 h of fasting from the tail vein. Serum was obtained after 10 min centrifugation (3000 rpm) at 4 °C. The Ultra Sensitive Mouse Insulin ELISA Kit (Crystal Chem Inc, IL, USA, 90080), the Serum Triglyceride Determination Kit (Sigma-Aldrich, TR0100-1 KT), the Cholesterol Kit (Biosystems, Spain, 11505), NEFAs kit (Wako Diagnostic, 434–91795, 436–91995, 270–77000), and Mouse ELISA leptin ELISA kit (Sigma, RAB0334) were used to measure the levels of insulin, triglyceride, cholesterol, NEFAs and leptin, respectively, according to the manufacturer's instructions. HDL cholesterol levels were measured in the supernatant obtained after the precipitation of serum VLDL and LDL particles with 0.44 mmol/L phosphotungstic acid (Merck, Darmstadt, Germany) and 20 mmol/L magnesium chloride (Sigma-Aldrich Chemie, Taufkirchen, Germany). HDL cholesterol and free glycerol levels were measured by using enzymatic colorimetric assays (Roche and Sigma-Aldrich Chemie, Taufkirchen, Germany) adapted to a COBAS 6000 autoanalyzer. VLDL and LDL cholesterol levels were measured by subtracting HDL cholesterol from the total cholesterol (Cedó et al., 2020).

4.15. Lipid extraction and thin layer chromatography of liver and adipose tissues

Lipids were extracted as previously described (Cal et al., 2012; Barriga et al., 2013), with minor modifications. One aliquot of pulverized tissue (10 mg for liver, eWAT and iWAT, or 5 mg for BAT) was homogenized in 1 ml or 0.5 ml of 0.1 M NaOH, respectively. In adipose tissues, a dilution 1:100 was used for extraction. Then, dichloromethane:methanol mixture (1:2) (3 ml) was added to the homogenate followed by addition of dichloromethane (1 ml) and centrifuged at 3500 rpm for 15 min to obtain the organic phase. Free cholesterol and TG content present in the lipid extract was analyzed by thin layer chromatography (TLC). Once the organic solvent was removed under a N_2 stream, the lipid extract was redissolved in dichloromethane and loaded onto silica chromatography plates (DC-Fertigplatten SIL G-25UV, Macherey-Nagel). The standards (a mixture of cholesterol, cholesterol palmitate, and triglycerides) were applied to each plate in order to localize the corresponding bands. The chromatographic developing solution was heptane/diethylether/acetic acid (74:21:4, v/v/v). Plates were stained with a solution of 5% phosphomolybdic acid and 5% sulfuric acid in ethanol and heated at 100 °C for 7 min. Spots corresponding to TG and free cholesterol according to the standards were quantified by densitometry using a Chemidoc XRC (Bio-Rad).

4.16. Histological analysis

After the sacrifice, samples of iBAT, iWAT, gWAT, liver and Matrigel pad from each mouse were immersed in 10% formalin for 24 h. Then, fatty tissues and Matrigel pads were transferred to 1X DPBS and the liver to 50% ethanol. Finally, they were sent to the Histology Service of the Animal Experimentation Unit of the School of Medicine, University of Barcelona, for processing. The samples were dehydrated and paraffin-embedded, cut into 4-μm sections and stained with hematoxylin and eosin (H&E).

Two-four μm thickness sections from paraffin embedded samples were used for immunohistochemistry at the Tumour Bank of the HCB-IDIBAPS Biobank (IDIBAPS, Barcelona) using the Leica Microsystems' Bond-max™ automated immunostainer together with the Bond Polymer Refine Detection System (Leica Microsystems, Spain). Briefly, tissue sections were depparafinized, and pretreated for antigen retrieval with 1 mM EDTA, pH 8.0 15 min for CD3 or with citrate buffer, pH 6.0 20 min for Mac2 and Caspase3. For macrophage immunostaining: primary monoclonal rat anti-murine antibody to Mac2 (Cedarlane, ON, Canada, CL8942, clone M3/38) was used at 1:40,000 for 1 h, combined with a secondary rabbit anti-rat Ig at 1:3000. For T cells staining: primary polyclonal rabbit anti-murine CD3 antibody (Cell Marque, CA, USA, CMC10317022) was used at 1:4000 for 2 h. For apoptosis: monoclonal rabbit anti-murine Caspase3 antibody (Cell Signaling, MA, USA, 9664) at 1:500 for 1 h. Finally, samples were developed with diaminobenzidine and counterstained with hematoxylin. Images of the stained samples were taken using a microscope (Leica DMI4000 B and Leica DFC300 FX camera) and processed with the Fiji ImageJ1.33 software (NIH; Bethesda, MD, USA).

4.17. CPT1 activity

Mitochondria-enriched fractions were obtained from LV-infected AT-MSCs-derived adipocytes grown in 10-cm2 dishes, and CPT1 activity was measured with 25μg/point by a radiometric method as described (Herrero et al., 2005a).

4.18. FA oxidation

Total oleate oxidation was measured in LV-infected AT-MSCs-derived adipocytes grown in 12-well plates. The day of the assay, cells were washed in KRBH-0.1% BSA, preincubated at 37 °C for 30 min in KRBH-1% BSA and washed again in KRBH-0.1% BSA. Cells were then incubated for 3 h at 37 °C with 320 μl/well of fresh KRBH containing 11 mM glucose, 0.8 mM carnitine, and 0.2 mM [1–14C]oleate (PerkinElmer, MA, USA). Oxidation was measured as described before with minor modifications (Orellana-Gavaldà et al., 2011). Plates were tightly sealed with parafilm. To stop the reaction, 40 μl/well of 40% HClO3 were added with a 1 mL syringe. Sealed plates were left o/n at room temperature. To measure the acid soluble products (ASPs), the incubation media was centrifuged at 14,000 rpm for 10 min and 150 μl of the supernatant were quantified. The scintillation values were normalized to the protein content of each well. Total oleate oxidation is represented as the sum of the oxidation to CO_2 plus ASPs.

4.19. Bioinformatics and statistical analysis

Data are expressed as the mean ± standard error of the mean (SEM). Student's t-test was used when two groups were compared. Dunnett's test was performed when several groups were compared to the control group. One-way ANOVA followed by Tukey's post-hoc test was used when one variable was compared between more than two groups. To compare two variables, we performed two-way ANOVA followed by Šidák or Tukey's post-hoc test for multiple comparison correction between two groups or more than two groups, respectively. Differences were considered statistically significant when the level of confidence was above 95% (P value < 0.05). All statistical analyses and figures were performed and generated using GraphPad Prism 8.0.2 (GraphPad Software, La Jolla, CA, USA). Adipocyte area was calculated with the MRI Adipocytes Tools of ImageJ.

Author contribution

MCS-V, NC, AC, DS and LH conceived the project. MCS-V, MR, MT, KD, CC, AB-A, MTLL, PM, SZ, MB-P, KI and JCE-G performed the experiments and analyzed the data under the supervision of JCE-G, VLl-C, AC, DS and LH. MCS-V and LH wrote the manuscript and designed the figures. JCE-G, VLl-C, AC, DS and LH provided funding.

Declaration of interests statement

The authors declare no conflicts of interest.

Data availability

Data will be made available on request.

Acknowledgements

This study was supported by the Spanish Ministry of Science and Innovation (MCIN/AEI) (SAF2017-83813-C3-1-R and PID2020-114953RB-C21 to LH and DS and PID2019-108792GB-I00 supported by MCIN/AEI/10.13039/501100011033 and PDC2021-121051-I00 to AC, co-funded by the European Regional Development Fund [ERDF]), the Biomedical Research Centre in Pathophysiology of Obesity and Nutrition (CIBEROBN) (Grant CB06/03/0001 to LH), the Merck Health Foundation (to LH), the Government of Catalonia (2017SGR278 to DS and 2021SGR00367 to LH), the ERC-2020-PoC to AC, the Marató de TV3 Foundation (201627–30 to DS and 202012–32 to AC) and FIS PI21/01523 (to VLl-C), from Fundación BBVA *Ayudas a equipos de investigación* 2019 ("Translational Molecular Imaging for Detection of Cholesterol Entrapment in the Vasculature with 68Ga-labeled LRP1-derived Peptides" to VLl-C). VLl-C and JCE-G are part of CIBER Enfermedades Cardiovasculares (CIBERCV; CB16/11/00276) and CIBERDEM (CB07/08/0016), respectively, run by the Instituto de Salud Carlos III. MS-V is a recipient of the *Ajut de Personal Investigador Predoctoral en Formació* (APIF) doctoral fellowship from the University of Barcelona. AC is a recipient of an ICREA "Academia" Award (Generalitat de Catalunya). AB-A is a fellow granted by the Program (FI19/00205) *Contratos predoctorales de formación de investigación en salud* from the Instituto de Salud Carlos III (ISCIII) and co-financed with ERDFs. The authors thank Senda Jiménez-Delgado for helping with the molecular work.

Appendix A. Supplementary data

Supplementary data to this article can be found online at https://doi.org/10.1016/j.ymben.2023.04.010.

References

Alcalá, M., Calderon-Dominguez, M., Bustos, E., Ramos, P., Casals, N., Serra, D., Viana, M., Herrero, L., 2017. Increased inflammation, oxidative stress and mitochondrial respiration in brown adipose tissue from obese mice. Sci. Rep. 7, 16082.

Barbagallo, I., Li Volti, G., Galvano, F., Tettamanti, G., Pluchinotta, F.R., Bergante, S., Vanella, L., 2017. Diabetic human adipose tissue-derived mesenchymal stem cells fail to differentiate in functional adipocytes. Exp. Biol. Med. 242, 1079–1085.

Barriga, M., Cal, R., Cabello, N., Llach, A., Vallmitjana, A., Benítez, R., Badimon, L., Cinca, J., Llorente-Cortés, V., Hove-Madsen, L., 2013. Low density lipoproteins promote unstable calcium handling accompanied by reduced SERCA2 and connexin-40 expression in cardiomyocytes. PLoS One 8, e58128.

Bastías-Pérez, M., Zagmutt, S., Soler-Vázquez, M.C., Serra, D., Mera, P., Herrero, L., 2020. Impact of adaptive thermogenesis in mice on the treatment of obesity. Cells 9, 316.

Bruce, C.R., Hoy, A.J., Turner, N., Watt, M.J., Allen, T.L., Carpenter, K., Cooney, G.J., Febbraio, M. a, Kraegen, E.W., 2009. Overexpression of carnitine palmitoyltransferase-1 in skeletal muscle is sufficient to enhance fatty acid oxidation and improve high-fat diet-induced insulin resistance. Diabetes 58, 550–558.

Cai, J., Jiang, S., Quan, Y., Lin, J., Zhu, S., Wang, J., Jiang, W., Liao, Y., Lu, F., 2022. Skeletal muscle provides a pro-browning microenvironment for transplanted brown adipose tissue to maintain its effect to ameliorate obesity in ob/ob mice. Faseb. J. 36, e22056.

Cal, R., Castellano, J., Revuelta-López, E., Aledo, R., Barriga, M., Farré, J., Vilahur, G., Nasarre, L., Hove-Madsen, L., Badimon, L., et al., 2012. Low-density lipoprotein receptor-related protein 1 mediates hypoxia-induced very low density lipoprotein-cholesteryl ester uptake and accumulation in cardiomyocytes. Cardiovasc. Res. 94, 469–479.

Calderon-Dominguez, M., Mir, J.F., Fucho, R., Weber, M., Serra, D., Herrero, L., 2016a. Fatty acid metabolism and the basis of brown adipose tissue function. Adipocyte 5, 98–118.
Calderon-Dominguez, M., Sebastián, D., Fucho, R., Weber, M., Mir, J.F., García-Casarrubios, E., Obregón, M.J., Zorzano, A., Valverde, Á.M., Serra, D., et al., 2016b. Carnitine palmitoyltransferase 1 increases lipolysis, UCP1 protein expression and mitochondrial activity in Brown adipocytes. PLoS One 11, e0159399.
Calvo, E., Keiran, N., Núñez-Roa, C., Maymó-Masip, E., Ejarque, M., Sabadell-Basallote, J., Del Mar Rodríguez-Peña, M., Ceperuelo-Mallafré, V., Seco, J., Benaiges, E., et al., 2021. Effects of stem cells from inducible brown adipose tissue on diet-induced obesity in mice. Sci. Rep. 11, 13923.
Camino, T., Lago-Baameiro, N., Martis-Sueiro, A., Couto, I., Santos, F., Baltar, J., Pardo, M., 2020. Deciphering adipose tissue extracellular vesicles protein cargo and its role in obesity. Int. J. Mol. Sci. 21, 1–16.
Cannon, B., Nedergaard, J., 2004. Brown adipose tissue: function and physiological significance. Physiol. Rev. 84, 277–359.
Casals, N., Zammit, V., Herrero, L., Fadó, R., Rodríguez-Rodríguez, R., Serra, D., 2016. Carnitine palmitoyltransferase 1C: from cognition to cancer. Prog. Lipid Res. 61, 134–148.
Cedó, L., Metso, J., Santos, D., García-León, A., Plana, N., Sabate-Soler, S., Rotllan, N., Rivas-Urbina, A., Méndez-Lara, K.A., Tondo, M., et al., 2020. LDL receptor regulates the reverse transport of macrophage-derived unesterified cholesterol via concerted action of the HDL-LDL Axis: insight from mouse models. Circ. Res. 127, 778–792.
Chen, L., Wang, L., Li, Y., Wuang, L., Liu, Y., Pang, N., Luo, Y., He, J., Zhang, L., Chen, N., et al., 2018. Transplantation of normal adipose tissue improves blood flow and reduces inflammation in high fat fed mice with hindlimb ischemia. Front. Physiol. 9, 197.
Conley, S.M., Hickson, L.J., Kellogg, T.A., Mckenzie, T., Heimbach, J.K., Taner, T., Tang, H., Jordan, K.L., Saadiq, I.M., Woollard, J.R., et al., 2020. Human obesity induces dysfunction and early senescence in adipose tissue-derived mesenchymal stromal. Stem Cell. 8, 1–11.
Cramer, C., Freisinger, E., Jones, R.K., Slakey, D.P., Dupin, C.L., Newsome, E.R., Alt, E. U., Izadpanah, R., 2010. Persistent high glucose concentrations alter the regenerative potential of mesenchymal stem cells. Stem Cell. Dev. 19, 1875–1884.
Crewe, C., Scherer, P.E., 2022. Intercellular and interorgan crosstalk through adipocyte extracellular vesicles. Rev. Endocr. Metab. Disord. 23, 61–69.
Cypess, A.M., Lehman, S., Williams, G., Tal, I., Rodman, D., Goldfine, A.B., Kuo, F.C., Palmer, E.L., Tseng, Y.H., Doria, A., et al., 2009. Identification and importance of brown adipose tissue in adult humans. N. Engl. J. Med. 360, 1509–1517.
de Mello, A.H., Costa, A.B., Engel, J.D.G., Rezin, G.T., 2018. Mitochondrial dysfunction in obesity. Life Sci. 192, 26–32.
Dominici, M., Blanc, K. Le, Mueller, I., Marini, F.C., Krause, D.S., Deans, R.J., Keating, A., Prockop, D.J., Horwitz, E.M., 2006. Minimal criteria for defining multipotent mesenchymal stromal cells. The International Society for Cellular Therapy position statement. Cytotherapy 8, 315–317.
Duscher, D., Rennert, R.C., Januszyk, M., Anghel, E., Maan, Z.N., Whittam, A.J., Perez, M.G., Kosaraju, R., Hu, M.S., Walmsley, G.G., et al., 2014. Aging disrupts cell subpopulation dynamics and diminishes the function of mesenchymal stem cells. Sci. Rep. 4, 1–9.
Fijany, A., Sayadi, L.R., Khoshab, N., Banyard, D.A., Shaterian, A., Alexander, M., Lakey, J.R.T., Paydar, K.Z., Evans, G.R.D., Widgerow, A.D., 2019. Mesenchymal stem cell dysfunction in diabetes. Mol. Biol. Rep. 46, 1459–1475.
Fink, T., Lund, P., Pilgaard, L., Rasmussen, J.G., Duroux, M., Zachar, V., 2008. Instability of standard PCR reference genes in adipose-derived stem cells during propagation, differentiation and hypoxic exposure. BMC Mol. Biol. 9, 98.
Follenzi, A., Sabatino, G., Lombardo, A., Boccaccio, C., Naldini, L., 2002. Efficient gene delivery and targeted expression to hepatocytes in vivo by improved lentiviral vectors. Hum. Gene Ther. 13, 243–260.
Gao, X., Li, K., Hui, X., Kong, X., Sweeney, G., Wang, Y., Xu, A., Teng, M., Liu, P., Wu, D., 2011. Carnitine palmitoyltransferase 1A prevents fatty acid-induced adipocyte dysfunction through suppression of c-Jun N-terminal kinase. Biochem. J. 435, 723–732.
Gavaldà-Navarro, A., Villarroya, J., Cereijo, R., Giralt, M., Villarroya, F., 2022. The endocrine role of brown adipose tissue: an update on actors and actions. Rev. Endocr. Metab. Disord. 23, 31–41.
Haemmerle, G., Zimmermann, R., Hayn, M., Theussl, C., Waeg, G., Wagner, E., Sattler, W., Magin, T.M., Wagner, E.F., Zechner, R., 2002. Hormone-sensitive lipase deficiency in mice causes diglyceride accumulation in adipose tissue, muscle, and testis. J. Biol. Chem. 277, 4806–4815.
Hany, T.F., Gharehpapagh, E., Kamel, E.M., Buck, A., Himms-Hagen, J., Von Schulthess, G.K., 2002. Brown adipose tissue: a factor to consider in symmetrical tracer uptake in the neck and upper chest region. Eur. J. Nucl. Med. 29, 1393–1398.
Hass, R., Kasper, C., Böhm, S., Jacobs, R., 2011. Different populations and sources of human mesenchymal stem cells (MSC): a comparison of adult and neonatal tissue-derived MSC. Cell Commun. Signal. 9, 12.
Herold, J., Kalucka, J., 2021. Angiogenesis in adipose tissue: the interplay between adipose and endothelial cells. Front. Physiol. 11.
Herrero, L., Rubí, B., Sebastián, D., Serra, D., Asins, G., Maechler, P., Prentki, M., Hegardt, F.G., 2005a. Alteration of the malonyl-CoA/carnitine palmitoyltransferase I interaction in the beta-cell impairs glucose-induced insulin secretion. Diabetes 54, 462–471.
Herrero, L., Rubí, B., Sebastián, D., Serra, D., Asins, G., Maechler, P., Prentki, M., Hegardt, F.G., 2005b. Alteration of the M alonyl- CoA/carnitine palmitoyltransferase I interaction in the β-cell impairs glucose-induced insulin secretion. Diabetes 54, 462–471.
Houmard, J.A., 2008. Intramuscular lipid oxidation and obesity. Am. J. Physiol. Regul. Integr. Comp. Physiol. 294, R1111–R1116.
Hristov, I., Mocanu, V., Zugun-Eloae, F., Labusca, L., Cretu-Silivestru, I., Oboroceanu, T., Tiron, C., Tiron, A., Burlacu, A., Pinzariu, A.C., et al., 2019. Association of intracellular lipid accumulation in subcutaneous adipocyte precursors and plasma adipokines in bariatric surgery candidates. Lipids Health Dis. 18, 1–8.
Jones, J.E.C., Rabhi, N., Orofino, J., Gamini, R., Perissi, V., Vernochet, C., Farmer, S.R., 2020. The adipocyte acquires a fibroblast-like transcriptional signature in response to a high fat diet. Sci. Rep. 10, 1–15.
Kelley, D.E., He, J., Menshikova, E.V., Ritov, V.B., 2002. Dysfunction of mitochondria in human skeletal muscle in type 2 diabetes. Diabetes 51, 2944–2950.
Kikai, M., Yamada, H., Wakana, N., Terada, K., Yamamoto, K., Wada, N., Motoyama, S., Saburi, M., Sugimoto, T., Irie, D., et al., 2017. Transplantation of brown adipose tissue inhibits atherosclerosis in apoE-/- mice: contribution of the activated FGF-21-adiponectin axis. Cardiovasc. Res. 114 (6), i1–i13.
Kishida, T., Ejima, A., Yamamoto, K., Tanaka, S., Yamamoto, T., Mazda, O., 2015. Reprogrammed functional Brown adipocytes ameliorate insulin resistance and dyslipidemia in diet-induced obesity and type 2 diabetes. Stem Cell Rep. 5, 569–581.
Kolaparthy, L.K., Sanivarapu, S., Moogla, S., Kutcham, R.S., 2015. Adipose tissue - adequate, accessible regenerative material. Int. J. Stem Cells 8, 121–127.
Kornicka, K., Houston, J., Marycz, K., 2018. Dysfunction of mesenchymal stem cells isolated from metabolic syndrome and type 2 diabetic patients as result of oxidative stress and autophagy may limit their potential therapeutic use. Stem Cell Rev. Reports 14, 337–345.
Lee, C.-W., Hsiao, W.-T., Lee, O.K.-S., 2017. Mesenchymal stromal cell-based therapies reduce obesity and metabolic syndromes induced by a high-fat diet. Transl. Res. 182, 61–74.e8.
Legzdina, D., Romanauska, A., Nikulshin, S., Kozlovska, T., Berzins, U., 2016. Characterization of senescence of culture-expanded human adipose-derived mesenchymal stem cells. Int. J. Stem Cells 9, 124–136.
Lin, D., Chun, T.-H., Kang, L., 2016. Adipose extracellular matrix remodelling in obesity and insulin resistance. Biochem. Pharmacol. 119, 8–16.
Liu, X., Zheng, Z., Zhu, X., Meng, M., Li, L., Shen, Y., Chi, Q., Wang, D., Zhang, Z., Li, C., et al., 2013. Brown adipose tissue transplantation improves whole-body energy metabolism. Cell Res. 23, 851–854.
Liu, X., Wang, S., You, Y., Meng, M., Zheng, Z., Dong, M., Lin, J., Zhao, Q., Zhang, C., Yuan, X., et al., 2015. Brown adipose tissue transplantation reverses obesity in ob/ob mice. Endocrinology 156, 2461–2469.
Liu, M., Lei, H., Dong, P., Fu, X., Yang, Z., Yang, Y., Ma, J., Liu, X., Cao, Y., Xiao, R., 2017. Adipose-derived mesenchymal stem cells from the elderly exhibit decreased migration and differentiation abilities with senescent properties. Cell Transplant. 26, 1505–1519.
Lu, K.Y., Primus Dass, K.T., Lin, S.Z., Harn, H.J., Liu, S.P., 2020. The application of stem cell therapy and brown adipose tissue transplantation in metabolic disorders. Cytotherapy 22, 521–528.
Malandrino, M.I., Fucho, R., Weber, M., Calderon-Dominguez, M., Mir, J.F., Valcarcel, L., Escoté, X., Gómez-Serrano, M., Peral, B., Salvadó, L., et al., 2015. Enhanced fatty acid oxidation in adipocytes and macrophages reduces lipid-induced triglyceride accumulation and inflammation. Am. J. Physiol. Metab. 308, E756–E769.
Mastrolia, I., Foppiani, E.M., Murgia, A., Candini, O., Samarelli, A.V., Grisendi, G., Veronesi, E., Horwith, E.M., Dominici, M., 2019. Challenges in clinical development of mesenchymal stromal/stem cells: concise review. Stem Cells Transl. Med. 8, 1135–1148.
McGarry, J.D., Mills, S.E., Long, C.S., Foster, D.W., 1983. Observations on the affinity for carnitine, and malonyl-CoA sensitivity, of carnitine palmitoyltransferase I in animal and human tissues. Demonstration of the presence of malonyl-CoA in non-hepatic tissues of the rat. Biochem. J. 214, 21–28.
Min, S.Y., Kady, J., Nam, M., Rojas-Rodriguez, R., Berkenwald, A., Kim, J.H., Noh, H.-L., Kim, J.K., Cooper, M.P., Fitzgibbons, T., et al., 2016. Human “brite/beige” adipocytes develop from capillary networks, and their implantation improves metabolic homeostasis in mice. Nat. Med. 22, 312–318.
Mir, J.F., Zagmutt, S., Lichtenstein, M.P., García-Villoria, J., Weber, M., Gracia, A., Fabriàs, G., Casas, J., López, M., Casals, N., et al., 2018. Ghrelin causes a decline in GABA release by reducing fatty acid oxidation in cortex. Mol. Neurobiol. 55, 7216–7228.
Monsénégo, J., Mansouri, A., Akkaoui, M., Lenoir, V., Esnous, C., Fauveau, V., Tavernier, V., Girard, J., Prip-Buus, C., 2012. Enhancing liver mitochondrial fatty acid oxidation capacity in obese mice improves insulin sensitivity independently of hepatic steatosis. J. Hepatol. 56, 632–639.
Morillas, M., Gómez-Puertas, P., Bentebibel, A., Sellés, E., Casals, N., Valencia, A., Hegardt, F.G., Asins, G., Serra, D., 2003. Identification of conserved amino acid residues in rat liver carnitine palmitoyltransferase I critical for malonyl-CoA inhibition. Mutation of methionine 593 abolishes malonyl-CoA inhibition. J. Biol. Chem. 278, 9058–9063.
Mushahary, D., Spittler, A., Kasper, C., Weber, V., Charwat, V., 2017. Isolation, cultivation, and characterization of human mesenchymal stem cells. Cytom. Part A 19–31.
Nahmgoong, H., Jeon, Y.G., Park, E.S., Choi, Y.H., Han, S.M., Park, J., Ji, Y., Sohn, J.H., Han, J.S., Kim, Y.Y., et al., 2022. Distinct properties of adipose stem cell subpopulations determine fat depot-specific characteristics. Cell Metabol. 34, 458–472.e6.
Nedergaard, J., Bengtsson, T., Cannon, B., 2007. Unexpected evidence for active brown adipose tissue in adult humans. Am. J. Physiol. Endocrinol. Metab. 293, E444–E452.
Neuhuber, B., Swanger, S.A., Howard, L., Mackay, A., Fischer, I., 2009. Effects of plating density and culture time on bone marrow stromal cell characteristics. Exp. Hematol. 36, 1176–1185.

Oguri, Y., Fujita, Y., Abudukadier, A., Ohashi, A., Goto, T., Furuya, F., Obara, A., Fukushima, T., Matsuo, N., Kim, M., et al., 2017. Tetrahydrobiopterin activates brown adipose tissue and regulates systemic energy metabolism. JCI Insight 2, 1–19.
Orellana-Gavaldà, J.M., Herrero, L., Malandrino, M.I., Pañeda, A., Sol Rodríguez-Peña, M., Petry, H., Asins, G., Van Deventer, S., Hegardt, F.G., Serra, D., 2011. Molecular therapy for obesity and diabetes based on a long-term increase in hepatic fatty-acid oxidation. Hepatology 53, 821–832.
O'Neill, S., O'Driscoll, L., 2015. Metabolic syndrome: a closer look at the growing epidemic and its associated pathologies. Obes. Rev. 16, 1–12.
Payab, M., Abedi, M., Foroughi Heravani, N., Hadavandkhani, M., Arabi, M., Tayanloo-Beik, A., Sheikh Hosseini, M., Gerami, H., Khatami, F., Larijani, B., et al., 2020. Brown adipose tissue transplantation as a novel alternative to obesity treatment: a systematic review. Int. J. Obes. 1–13.
Perdomo, G., Commerford, S.R., Richard, A.-M.T., Adams, S.H., Corkey, B.E., O'Doherty, R.M., Brown, N.F., 2004. Increased β-oxidation in muscle cells enhances insulin-stimulated glucose metabolism and protects against fatty acid-induced insulin resistance despite intramyocellular lipid accumulation. J. Biol. Chem. 279, 27177–27186.
Petrovic, N., Walden, T.B., Shabalina, I.G., Timmons, J.A., Cannon, B., Nedergaard, J., 2010. Chronic peroxisome proliferator-activated receptor γ (PPARγ) activation of epididymally derived white adipocyte cultures reveals a population of thermogenically competent, UCP1-containing adipocytes molecularly distinct from classic brown adipocytes. J. Biol. Chem. 285, 7153–7164.
Rennert, R.C., Sorkin, M., Januszyk, M., Duscher, D., Kosaraju, R., Chung, M.T., Lennon, J., Radiya-Dixit, A., Raghvendra, S., Maan, Z.N., et al., 2014. Diabetes impairs the angiogenic potential of adipose-derived stem cells by selectively depleting cellular subpopulations. Stem Cell Res. Ther. 5, 1–12.
Riis, S., Zachar, V., Boucher, S., Vemuri, M.C., Pennisi, C.P., Fink, T., 2015. Critical steps in the isolation and expansion of adipose-derived stem cells for translational therapy. Expet Rev. Mol. Med. 17.
Ritov, V.B., Menshikova, E.V., He, J., Ferrell, R.E., Goodpaster, B.H., Kelley, D.E., 2005. Deficiency of subsarcolemmal mitochondria in obesity and type 2 diabetes. Diabetes 54, 8–14.
Rojas-Rodriguez, R., Lujan-Hernandez, J., Min, S.Y., DeSouza, T., Teebagy, P., Desai, A., Tessier, H., Slamin, R., Siegel-Reamer, L., Berg, C., et al., 2019. Generation of functional human adipose tissue in mice from primed progenitor cells. Tissue Eng. A 25, 842–854.
Saito, M., Okamatsu-Ogura, Y., Matsushita, M., Watanabe, K., Yoneshiro, T., Nio-Kobayashi, J., Iwanaga, T., Miyagawa, M., Kameya, T., Nakada, K., et al., 2009. High incidence of metabolically active brown adipose tissue in healthy adult humans: effects of cold exposure and adiposity. Diabetes 58, 1526–1531.
Seale, P., Kajimura, S., Yang, W., Chin, S., Rohas, L., Tavernier, G., Langin, D., Spiegelman, B.M., 2007. Transcriptional control of brown fat determination by PRDM16. Cell Metabol. 6, 38–54.
Seale, P., Conroe, H.M., Estall, J., Kajimura, S., Frontini, A., Ishibashi, J., Cohen, P., Cinti, S., Spiegelman, B.M., 2011. Prdm16 determines the thermogenic program of subcutaneous white adipose tissue in mice. J. Clin. Invest. 121, 96–105.
Sebastián, D., Herrero, L., Serra, D., Asins, G., Hegardt, F.G., 2007. CPT I overexpression protects L6E9 muscle cells from fatty acid-induced insulin resistance. Am. J. Physiol. Endocrinol. Metab. 292, E677–E686.
Serra, D., Mera, P., Malandrino, M.I., Mir, J.F., Herrero, L., 2013. Mitochondrial fatty acid oxidation in obesity. Antioxidants Redox Signal. 19, 269–284.
Shankar, K., Kumar, D., Gupta, S., Varshney, S., Rajan, S., Srivastava, A., Gupta, A., Gupta, A.P., Vishwakarma, A.L., Gayen, J.R., et al., 2019. Role of brown adipose tissue in modulating adipose tissue inflammation and insulin resistance in high-fat diet fed mice. Eur. J. Pharmacol. 854, 354–364.
Silva, K.R., Baptista, L.S., 2019. Adipose-derived stromal/stem cells from different adipose depots in obesity development. World J. Stem Cell. 11, 147–166.
Silva, F.J., Holt, D.J., Vargas, V., Yockman, J., Boudina, S., Atkinson, D., Grainger, D.W., Revelo, M.P., Sherman, W., Bull, D. a, et al., 2014. Metabolically active human brown adipose tissue derived stem cells. Stem Cell. 32, 572–581.
Simoneau, J.A., Veerkamp, J.H., Turcotte, L.P., Kelley, D.E., 1999. Markers of capacity to utilize fatty acids in human skeletal muscle: relation to insulin resistance and obesity and effects of weight loss. Faseb. J. 13, 2051–2060.
Soler-Vázquez, M.C., Mera, P., Zagmutt, S., Serra, D., Herrero, L., 2018. New approaches targeting brown adipose tissue transplantation as a therapy in obesity. Biochem. Pharmacol. 155, 346–355.
Stanford, K.I., Middelbeek, R.J.W., Townsend, K.L., An, D., Nygaard, E.B., Hitchcox, K. M., Markan, K.R., Nakano, K., Hirshman, M.F., Tseng, Y.-H., et al., 2013. Brown adipose tissue regulates glucose homeostasis and insulin sensitivity. J. Clin. Invest. 123, 215–223.
Stefanovic-Racic, M., Perdomo, G., Mantell, B.S., Sipula, I.J., Brown, N.F., O'Doherty, R. M., 2008. A moderate increase in carnitine palmitoyltransferase 1a activity is sufficient to substantially reduce hepatic triglyceride levels. Am. J. Physiol. Endocrinol. Metab. 294, E969–E977.
Thoonen, R., Ernande, L., Cheng, J., Nagasaka, Y., Miranda-bezerra, A., Chen, C., Chao, W., Panagia, M., David, E., Puppala, D., et al., 2016. Functional Brown Adipose Tissue Limits Cardiomyocyte Injury and Adverse Remodeling in Catecholamine-Induced Cardiomyopathy, pp. 202–211.
Ussar, S., Lee, K.Y., Dankel, S.N., Boucher, J., Haering, M.F., Kleinridders, A., Thomou, T., Xue, R., Macotela, Y., Cypess, A.M., et al., 2014. ASC-1, PAT2, and P2RX5 are cell surface markers for white, beige, and brown adipocytes. Sci. Transl. Med. 6.
van Marken Lichtenbelt, W.D., Vanhommerig, J.W., Smulders, N.M., Drossaerts, J.M. a F. L., Kemerink, G.J., Bouvy, N.D., Schrauwen, P., Teule, G.J.J., 2009. Cold-activated Brown Adipose Tissue in Healthy Men.
Virtanen, K.A., Lidell, M.E., Orava, J., Heglind, M., Westergren, R., Niemi, T., Taittonen, M., Laine, J., Savisto, N.-J., Enerbäck, S., et al., 2009. Functional brown adipose tissue in healthy adults. N. Engl. J. Med. 360, 1518–1525.
Vitali, A., Murano, I., Zingaretti, M.C., Frontini, A., Ricquier, D., Cinti, S., 2012. The adipose organ of obesity-prone C57BL/6J mice is composed of mixed white and brown adipocytes. J. Lipid Res. 53, 619–629.
Weber, M., Mera, P., Casas, J., Salvador, J., Rodríguez, A., Alonso, S., Sebastián, D., Soler-Vázquez, M.C., Montironi, C., Recalde, S., et al., 2020. Liver CPT1A gene therapy reduces diet-induced hepatic steatosis in mice and highlights potential lipid biomarkers for human NAFLD. Faseb. J. 34, 11816–11837.
White, J.D., Dewal, R.S., Stanford, K.I., 2019. The beneficial effects of brown adipose tissue transplantation. Mol. Aspect. Med. 68, 74–81.
Williams, D.M., Nawaz, A., Evans, M., 2020. Drug therapy in obesity: a review of current and emerging treatments. Diabetes Ther. 11, 1199–1216.
Wu, R., Liu, X.M., Sun, J.G., Chen, H., Ma, J., Dong, M., Peng, S., Wang, J.Q., Ding, J.Q., Li, D.H., et al., 2017. DJ-1 maintains energy and glucose homeostasis by regulating the function of brown adipose tissue. Cell Discov. 3, 1–18.
Yuan, X., Hu, T., Zhao, H., Huang, Y., Ye, R., Lin, J., Zhang, C., Zhang, H., Wei, G., Zhou, H., et al., 2016. Brown adipose tissue transplantation ameliorates polycystic ovary syndrome. Proc. Natl. Acad. Sci. USA 113, 2708–2713.
Zhang, F., Hao, G., Shao, M., Nham, K., An, Y., Wang, Q., Zhu, Y., Kusminski, C.M., Hassan, G., Gupta, R.K., et al., 2018. An adipose tissue atlas: an image-guided identification of human-like BAT and beige depots in rodents. Cell Metabol. 27, 252–262.e3.
Zhao, H., Shang, Q., Pan, Z., Bai, Y., Li, Z., Zhang, H., Zhang, Q., Guo, C., Zhang, L., Wang, Q., 2018. Exosomes from adipose-derived stem cells attenuate adipose inflammation and obesity through polarizing M2 macrophages and beiging in white adipose tissue. Diabetes 67, 235–247.
Zhu, Z., Spicer, E.G., Gavini, C.K., Goudjo-Ako, A.J., Novak, C.M., Shi, H., 2014. Enhanced sympathetic activity in mice with brown adipose tissue transplantation (transBATation). Physiol. Behav. 125, 21–29.
Zingaretti, M.C., Crosta, F., Vitali, A., Guerrieri, M., Frontini, A., Cannon, B., Nedergaard, J., Cinti, S., 2009. The presence of UCP1 demonstrates that metabolically active adipose tissue in the neck of adult humans truly represents brown adipose tissue. Faseb. J. 23, 3113–3120.
Zuriaga, M.A., Fuster, J.J., Gokce, N., Walsh, K., 2017. Humans and mice display opposing patterns of "browning" gene expression in visceral and subcutaneous white adipose tissue depots. Front. Cardiovasc. Med. 4, 1–5.